OSL Dating of a Woodland Period Occupation at the Hare Hammock Ring and Mound Complex, Bay County, Florida

By ALEX HODSON, B.Sc.

A Thesis Submitted to the School of Graduate Studies in Partial Fulfillment of the Requirements for the Degree Master of Science

McMaster University MASTER OF SCIENCE (2015) Hamilton, Ontario (Earth Sciences)

TITLE: **OSL Dating of a Woodland Period Occupation at the Hare Hammock Ring and Mound Complex, Bay County, Florida**
AUTHOR: Hodson, A.D. (McMaster University)
SUPERVISOR: Professor W.J. Rink
NUMBER OF PAGES: 58

ABSTRACT

This study used OSL dating to examine the chronological relationship between two adjacent archaeological sites at the Hare Hammock complex in northwest Florida. High-resolution vertical sampling was performed at 10cm intervals in profiles, one corresponding to a Swift Creek burial mound, and the other to a Weeden Island ring midden. This was done in order to determine the timing of occupations at the sites and look for patterns in radiation dosimetry. The Swift Creek mound was found to have a mean OSL age of 1835 +/- 68 years, consistent with archaeological expectations of the site and the accepted range of Swift Creek culture. The subsequent Weeden Island occupation was also found to have OSL ages within expectations, with a mean age of 1049 +/- 43 years that overlies a single age of 1511 +/- 372 years, corresponding to the Late and Early Weeden Island periods, respectively. The general coherence with radiocarbon dates and ceramic chronologies affirms the veracity of these OSL ages, which were obtained using a very recently developed dosimetric technique that applies Al_2O_3:C cylinders as in-situ dosimeters. These dosimeters indicated that the sediments at Hare Hammock contain significant heterogeneity in beta dose rates. This study finds that, under these circumstances, the best age results are obtained when applying the refined dosimetric technique which combines the beta dose rate from NAA/DNC and gamma dose rate from Al_2O_3:C dosimetry.

ACKNOWLEDGEMENTS

I would first like to thank Dr. Jack Rink for supervising this MSc thesis, and for the plentiful support and guidance he provided throughout this research. His suggestions and comments during both research and writing were of immeasurable aid to the development and completion of this thesis. I also thank several others who contributed their time and knowledge, including Mike Russo and Craig Dengel for their fieldwork and archaeological expertise. Dr. Regina DeWitt is thanked for her critical contribution of the Al_2O_3:C dosimeters and the analysis of their measurements. I would also like to thank Robert Hendricks and Kathleen Rodrigues for their assistance with sample preparation and additional discussions of results.

TABLE OF CONTENTS

LIST OF FIGURES

LIST OF TABLES

LIST OF EQUATIONS

Equation 1 The formula for OSL age calculation

LIST OF ABBREVIATIONS

a	Annum, years before present
Al_2O_3:C	Aluminum oxide
ASL	Above sea level
D_E	Equivalent dose
DNC	Delayed Neutron Counting
MAM3	3-Parameter Minimum Age Model
NAA	Neutron Activation Analysis
OSL	Optically Stimulated Luminescence
SAR	Single Aliquot Regenerative protocol
TAFB	Tyndall Air Force Base

CHAPTER 1: INTRODUCTION

1.1 Purpose and Significance of Study

The purpose of this study was to use OSL dating to analyze two adjacent archaeological sites with high-resolution vertical sampling. This high resolution OSL sampling was performed in order to determine the timing of occupations at the site, as well as to search for patterns in radiation dosimetry and post-depositional disturbance which can potentially compromise the integrity of OSL results. The significance of this work is that it provides for the first time OSL dating on a Weeden Island occupation, and for only the second time, on a Swift Creek occupation. Moreover, it is the first time that high resolution sampling has been used in the Weeden Island context. As such, it complements many other earlier studies using radiocarbon dating on a wide range of sites from these periods in the southeastern US, and provides direct comparisons against radiocarbon in this study. This study also tests a new application of in-situ Al_2O_3:C dosimeters by employing them for in-situ dosimetry use in conjunction with OSL. The use of Al_2O_3:C dosimetry in sedimentary environments is a very recent development, and this method has yet to be refined for use in sediments with beta dose rate heterogeneity. Using a combined approach of both in-situ Al_2O_3:C dosimetry and dosimetry based on neutron activation analysis (NAA) of small sub-samples, this study seeks to provide an understanding of the complex radiation environment that is a low dose rate sedimentary environment exhibiting beta dose rate heterogeneity. This comparison is used to determine how to most effectively apply these dosimetric techniques in heterogeneous sediments. This dosimetric approach also contributes to the significance of this study, since it is basically a new contribution to knowledge in dating archaeological sites in general, and because it has only been applied one other time to Woodland Period archaeology.

1.2 Previous Studies

1.2.1 Archaeological background

The first report on the 8By31 burial mound site at Hare Hammock was by Clarence B. Moore in 1902, who also performed an excavation of the Larger Mound (8By30) located approximately 400 yards (366 meters) northwest of the Smaller Mound (8By31). Moore identified vessels recovered from the Larger Mound which associate it with Weeden Island period (Willey, 1949). However, the Larger Mound held numerous burials (31), some of which are of the historic period, that were left unexcavated (Moore, 1902). Although the mound may have been used as a cemetery in historic times, this does not obviate its previous use as a Native American burial mound. Historical cemeteries would likely contain graves, nails, and soil disturbances, however, if the mound is a disturbed prehistoric mound, it should also contain artifacts originating from the periods during which it was constructed or in use by prehistoric Native Americans (Russo et al., 2014).

Had this been the end of Moore's excavations, the Smaller Mound construction at Hare Hammock would later likely have been related to Swift Creek culture, since the only diagnostic pottery recovered from the mound in 1902 would later be identified by Willey as Swift Creek series pottery, Hare Hammock Surface Indented. However, Moore returned in 1918 to excavate the area adjacent to the east side of the mound to search for the "pottery cache" since he had noticed this was a re-occurring burial pattern among many of the mounds in the region. This practice of disposing ceramics specifically on the east side of the mounds, which creates these "pottery caches", was later to be linked specifically to Weeden Island mounds (Russo et al., 2014). The east-side excavation produced ten whole vessels which included types that would later be classified by Willey as Weeden Island Incised and Tucker Ridge pinched, leading Willey to identify the mound as a Weeden Island I period construction (Russo et al., 2009). This interpretation is still considered ambiguous, especially since later archeologists expected to find evidence of Weeden Island mortuary, elite, and utilitarian pottery. However, exclusively Swift Creek pottery types were recovered from the mound proper. A generalized chronology of cultural periods in Florida is presented in Table 1.

Table 1. Generalized chronology of cultural periods in Florida (adapted from Milanich, 1994).

Period & Stage	Culture	Age	Age (years ago)
Early Woodland	Deptford	500 B.C. – 200 A.D.	2515 – 1815
Middle Woodland	Early Swift Creek	150 – 400 A.D.	1865 – 1615
	Late Swift Creek	400 – 800 A.D.	1615 - 1215
	Early Weeden Island	400 – 650 A.D.	1615 – 1365
Late Woodland	Late Weeden Island	650 – 1000 A.D.	1215 – 1015
Mississippian	Fort Walton	1000 – 1500 A.D.	1015 – 515

Ring middens were identified by Brose and Percy (1979) as the habitation sites associated with burial mounds in their model of Woodland period Native American settlement. These ring middens, comprised of animal bones, shells and fragments of non-descript pottery, are presumed to be constructed over time by the disposal of daily food waste and broken or unwanted pottery behind dwellings in a circular manner. Brose and Percy (1979), as well as others including Sears (1973), posited that the artifacts recovered from ring middens correspond to the secular aspects of society, while artifacts which had been placed in the burial mounds were more sacred. Apart from elaborate forms of pottery, sacred objects were also identified as objects which are made from rare, exotic, or high quality materials with a greater degree of craftsmanship. This includes groundstone celts, crystal quartz, ocher and mica objects, while secular objects were usually made from locally acquired common and low quality materials. Woodland period coastal dwellers in this region are hypothesized to have participated in the Hopewellian interaction sphere, a network and exchange and ceremony which connected distant communities across eastern North America (Moore 1902, 1918). This allowed them to obtain exotic and sacred objects which have little or no practical value, but have a substantial symbolic value. Such interactions helped to maintain relationships with

interior groups with whom coastal dwellers might take refuge during times of coastal subsistence stress (Russo, 2014). A number of the cultures known to have participated in the Hopewellian interaction sphere seem to have developed a socio-political hierarchy. Distinct sociological classes have become manifest in the archaeological record, as betokened by the burial of sacred and valuable objects next to high-status individuals in burial mounds (Milanich, 1994).

The Larger Hare Hammock Mound identified by Moore in 1902 contained an abundance of special mortuary wares, however Moore generally reported only the best of what he recovered, to the exclusion of most utilitarian wares. Unlike the larger mound, mortuary and sacred objects were scarce in the smaller Hare Hammock mound. In contrast to the scarcity of definitive sacred objects in the mound, the associated ring midden produced numerous reputed ritual objects, including effigy vessels, red ocher, ground stone caches, and crystal quartz. This suggests a reversal of sacred and secular contexts for these objects, a convention which has also been observed in other mounds and rings that have been studied in the region (Russo, 2014). Some of these mound and ring settlements, including the Hare Hammock complex, show evidence of an intriguing ritual occurring after the site's abandonment.

Despite the fact that the larger Weeden Island mound and ring settlement seems to have been occupied for centuries after abandonment of the neighbouring Swift Creek mound and ring (Harrison Ring), there is very little evidence of Weeden Island activity occurring at this earlier adjoining site. It seems the Weeden Island descendants refrained from using the older mound and ring site, with a single exception in a ritual context whereby a large cache of Weeden Island pottery was deposited adjacent to the east side of the Swift Creek mounds. This implies a sacralization of the ring and mound after the site was abandoned. An example of a similar distribution of pottery seems evident at Stranges Ring (Russo et al., 2012). The plaza at this site is surrounded by a semicircle of Middle Weeden Island utilitarian wares, with elite wares focused in a single location on the east side of the ring. Subsequent Wakulla Check stamped wares, which are not found within the ring, are distributed in a band surrounding it with the complete omission of any other kinds of pottery. This indicates that the Late Weeden Island descendants here seem to have generally avoided the reoccupation of the earlier ring. Although this hypothesis requires further investigation to verified, the evidence suggests that at least some of these Woodland period rings which began as occupation sites may have become sacred sites post-abandonment.

Mapping of mound and ring sites has also led to the discovery of a pattern in which the orientation of mounds to rings may have changed during the transition between the Swift Creek and Weeden Island cultures. Both placed mounds are located 20 and 50 meters away from their rings with a midden-free pathway in the ring facing the mound. Weeden Island Mounds, however, seem to have a consistent positioning relative to their rings, while this consistency in orientation is not manifested in the former Swift Creek

complexes. Weeden Island mounds were constructed on the northwest side of the rings, which is in the approximate position of the setting sun on the winter solstice relative to the center of the ring. The introduction of cardinal or celestial orientations in mound positioning after the appearance of Weeden Island ceramics is probably related to the Weeden Island predilection for celestial orientations as found at other interior mounds sites, on pottery, and the well-known east-side placement of caches.

The Hare Hammock and Harrison Ring sites, which can be considered one larger multicomponent mound and ring midden complex, has produced over two dozen radiocarbon dates which have provided archaeologists with an understanding of the site's development through time, as well as the chronology of related shifts between the Swift Creek and Weeden Island phases of occupation. The original Swift Creek ring midden (Harrison Ring) began to form around AD 400-500, as did the associated Smaller Hare Hammock Mound, and both of these continued to be used until around AD 675-725. At this point, which is contemporaneous with the appearance of Weeden Island prestige and mortuary wares, the larger Hare Hammock Ring midden began forming and the Larger Hare Hammock Mound was constructed. The previous ring midden and its mound were then abandoned, and the new larger ring midden and mound were occupied until around AD 1000. After this, Weeden Island ceramics are replaced in the record by Wakulla Checked Stamped pottery, which is distributed across the site but in a pattern which does conform with the earlier rings (Russo et al., 2014). An intriguing aspect of this chronology is the notably rapid shift from the old smaller ring and mound to the new larger ring and mound. This appears to have occurred within a couple of generations after the first appearance of Weeden Island prestige and mortuary ceramics.

1.2.2. Recent archaeological investigations at the Hare Hammock complex

A preliminary survey was conducted in 2007 by performing small excavations at the potential 8By31 site in an attempt to confirm the presence of the smaller mound at Hare Hammock reported by Moore. A systematic survey was also conducted at 20-meter intervals in the surrounding area. Two ring-midden sites were identified during these surveys, 8By1347 (Hare Hammock Ring) and 8By1359 (Harrison Ring) (Russo et al., 2009). The earliest of the small-scale investigations was reported by Russo and Dengel in 2009, with the most recent one conducted in 2013 which yielded a human bone from a shovel test. The identification of this bone as human was pivotal in ascertaining that the area in question does in fact represent the spoil of 8By31. The small size and poor preservation of the bone precluded the identification of its ethnicity, so the possibility remained that it originated from the conjectured nearby historic cemetery (Russo et al. 2009). As such, the bone material was authorized for radiocarbon dating and yielded an age of 1250 ± 60 years Cal BP, which is consistent with Late Swift Creek and confirms the presence of spoil from 8By31.

Human remains recovered from the Larger Hare Hammock Mound returned calibrated radiocarbon dates of 1160 ± 105 years CalBP and 1010 ± 120 years Cal BP, affirming the prehistoric age of both the human remains and the mound itself. These dates fall within the accepted range of Weeden Island cultures, although the earlier date could also be attributed to Late Swift Creek. Nonetheless, it appears that the hypothesis of the Larger mound as being a Weeden Island construction and the Smaller mound a Swift Creek construction based on examination of ceramics is supported by these radiocarbon dates.

At the two excavation units in Hare Hammock studied in this project, EU5 and EU6, most of the ceramics recovered have been classified as Swift Creek, with Weeden Island ceramics also present in EU6. Only three radiocarbon dates were yielded from these excavations, the results of which are listed in Table 2. The two dates from EU6 which are coeval with OSL samples are from residue and soot adhered to pottery sherds. The only date from EU5, however, comes from a sherd that was recovered from a layer which underlies the lowest OSL sample in the profile.

Table 2. Radiocarbon dates recovered from EU6 and EU5 (Russo et al., 2014)

Lab #	Unit/ level	Material	Artifact	Meas. age	$^{13}C/^{12}C$	Conve-ntional BP	Mean Cal BP	Cal AD 1 sigma	Cal AD 2 sigma
110-63.1[+]	EU6 L3	Residue	Wakulla CS	NA	NA	1205 ±15	1130	770-870	770-880
12013[#]	EU6 L4	Soot	Carrabelle P.	NA	-25.2	1210 ±25	1130	770-870	720-890
305250	EU5 L8	Residue	SCC Stamped	1540 ±30	-25.1	1540 ±30	1450	430-570	430-590

CS = Check Stamped; SCC = Swift Creek Complicated Stamped

1.3. Al_2O_3:C Dosimetry

Al_2O_3:C dosimeters have been well studied and applied for uses such as radiotherapy (eg. Botter-Jensen et al., 2003; Polf et al., 2003). These dosimeters have also been applied in sediments to determine dose-rate variation in samples by Kalchgruber et al. (2003), however only the full dose-rate could be determined by the dosimeters at the time. Kalchgruber and Wagner (2006) later refined the application of the Al_2O_3:C dosimeters by separating the beta and gamma dose rate components using a pair of dosimeters: one wrapped in thin foil which measures both the beta and gamma components, and a second packed in a copper container which measures only the gamma component. The beta component alone can thus be determined by taking the difference between the two dosimeters. This method of dosimetry has been applied to both homogenous and inhomogeneous sediments and successfully compared against results obtained using Ge- and on-site NaI-gamma dosimetry.

CHAPTER 2: STUDY AREA

2.1. Geographical Setting and Climate

The Hare Hammock Ring and mound complex is located in Tyndall Air Force Base (TAFB), which is situated on a 5 km wide peninsula between the Gulf of Mexico and East Bay, which is connected to St. Andrew Bay. (Figure 1). The maximum elevation of TAFB is less than 10 m ASL. The coast of this region is characterized by Holocene age barrier islands and sand spits. The site itself lays on the mainland peninsula and is separated from the Gulf of Mexico by two sandy spits (Crooked Island and Raffield Peninsula), which provide protection from storm activity. These also create a buffer for other coastal processes, so only small wind-blown dunes appear to be present. This region experiences long, warm and humid summers fairly mild winters (Duffee et al., 1984). Annual precipitation is usually about 60 inches, the bulk of which occurs between July and September, while October through to December is often much drier (Russo et al., 2009).

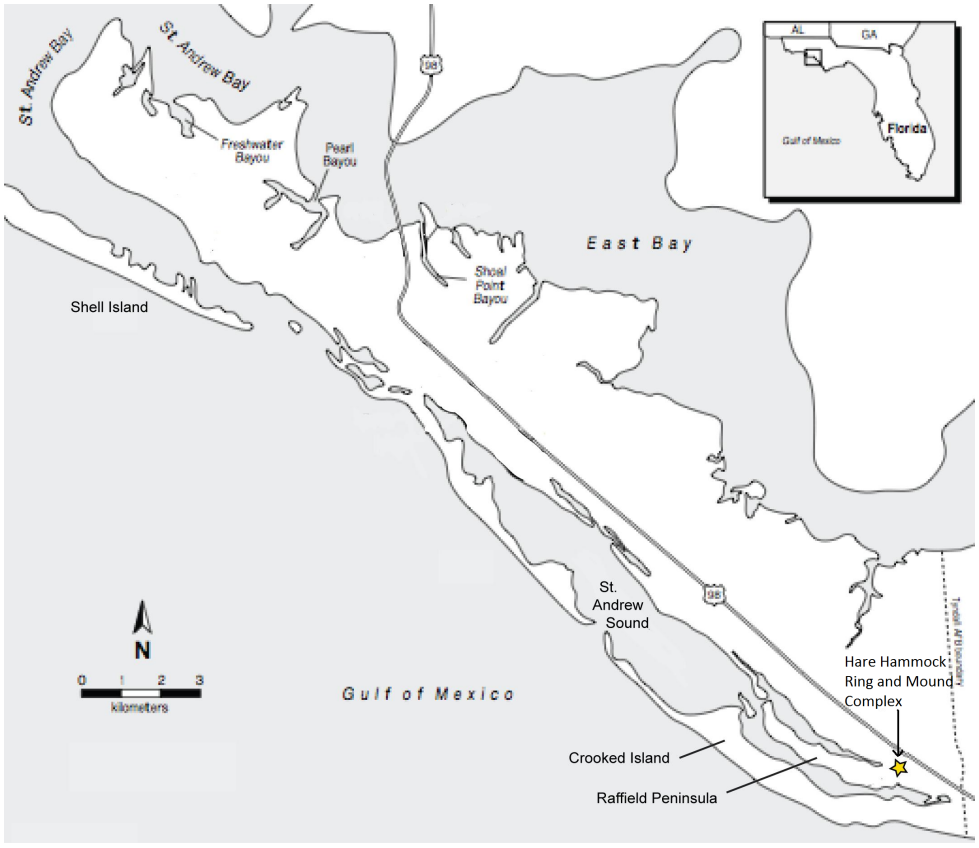

Figure 1. Regional map showing the location of the Hare Hammock Ring and Mound Complex (marked with a star) at Tyndall Air Force Base, Panama City, Florida (adapted from NOAA, 1997).

2.2. Archaeological Sites near Hare Hammock dated with OSL

There are a number of archaeological sites located near the coast in northwestern Florida. A few of these sites which are close to the Hare Hammock site have been dated using OSL. The closest of these is the neighbouring site of Harrison Ring, which was dated very recently by Rodrigues (2015) and is considered to be a connected part of the Hare Hammock complex. The other two sites, Richardson's Hammock and the Old Cedar site are both shell middens which have been successfully dated using OSL.

OSL sampling at Harrison Ring was performed on a sterile stratigraphic section which contained 40cm of archaeological horizons. Ages for these samples were obtained using single grain measurements, ranging from 1481 ± 286 years to 2114 ± 436 years. The uppermost and lowermost of these samples produced minimum ages of 1712 ± 321 years and 1481 ± 286 years, respectively. Despite this small apparent age inversion, when the errors are considered these results are statistically indistinguishable. An average of the single grain OSL ages from the four archaeological layers gives an approximate age for the occupation at this site of about 1751 ± 339 years ago. This result is consistent with the radiocarbon dates taken at Harrison Ring and the accepted chronology of Swift Creek culture. Furthermore, it re-enforces the archaeological evidence that this site was a Swift Creek occupation.

Richardson's Hammock, located at the southern end of St. Joseph Peninsula, was shown to be consistent with the accepted chronology of Early Weeden Island culture. The low overdispersion and skewness values reported by Lopez (2007) from this site indicate that the quartz was well bleached and probably unaffected by post-depositional disturbances. Not far north of Richardson's Hammock, the Old Cedar site produced an OSL age from the midden that correlates to the Late Weeden Island period, which is coherent with archaeological expectations derived from the ensemble of artifacts found at the site (Thompson et al., 2007). The samples from this site showed no distinctive evidence of incomplete bleaching or post-depositional disturbance, however, a small amount of positive skewness was present in the samples. Thompson et al. (2007) suggested that this could have been caused by natural variations resulting from dose rate inhomogeneities in the dose rate.

Similar circumstances were encountered in the sediments at Harrison Ring, where Al_2O_3:C dosimetry was used for the first time to demonstrate the high degree of variability in beta dose rates present in these sediments (Rodrigues, 2015). Using the combined technique of Al_2O_3:C dosimetry for gamma dose rates and NAA/DNC to calculate beta dose rates, single grain OSL ages were successfully determined and provide evidence that the site was occupied approximately 1751 ± 339 years ago. The samples here displayed high overdispersion and skewness, which was attributed mainly to the effects of beta-microdosimetry, with the potential of some post-depositional disturbance via bioturbation. Dose rates obtained from NAA/DNC and Al_2O_3:C dosimetry were

significantly different, highlighting the variability in beta dose rates. Ages calculated using the combined dosimetric technique were found to have best agreement with independent age control, which suggests that this is the most effective method of dosimetry to apply when dating sediments with a large heterogeneity in beta dose rates.

CHAPTER 3: INTRODUCTION TO LUMINESCENCE DATING

3.1. OSL Theory

3.1.1 Optically Stimulated Luminescence

Optically stimulated luminescence (OSL) is a natural phenomenon occurring in mineral grains which results from the ability of certain crystal structures to store energy from radiation and eventually release that energy as luminescence (Schwarcz, 2002). In nature, mineral grains are exposed to a constant dose of radiation sourced from radioactive isotopes in the surrounding environment (elements including uranium (U), thorium (Th) and potassium (K)) and from cosmic rays (Duller, 2008). In certain minerals, particularly quartz and feldspars, the energy received from the surrounding radiation is retained by the trapping of electrons which have been excited to metastable states and stored in defects in the crystal structure (Schwarcz, 2002). This accumulation of trapped charges provides a record of the amount of radiation that the mineral has been exposed to since the traps were last emptied (Feathers, 2003). The emptying of these traps is termed 'zeroing' or 'bleaching', and occurs when another energy source allows the trapped charges to escape and releases the accumulated energy as radiation (Duller, 2008). Bleaching is usually caused by exposure to sunlight or heating of the mineral above 300°C (Duller, 2008). Since bleaching removes all energy built up in a mineral, all of the energy which is retained by a mineral can be assumed to be a result of exposure to radiation after the bleaching event (Schwarcz, 2002). The accumulated energy referred to as the luminescence signal can therefore be used to estimate the age of the bleaching event (Feathers, 2003). This is done by dividing the strength of the natural luminescence signal, which is calculated as an equivalent dose (D_E), by an estimated annual dose rate (d) to obtain an approximate age (t), using the age equation:

$$t = D_E / d \qquad (1)$$

The ability to estimate the age of a bleaching event is significantly useful to both geologists and archaeologists for establishing chronologies, as it marks the date of either the burial or the heating of the given material (Schwarcz, 2002; Feathers, 2003). The method by which this age is determined is known as luminescence dating (Duller, 2008). The process of OSL luminescence involves exposing an isolated mineral, usually quartz, to radiation so that the luminescence signature can be measured (Schwarcz, 2002). Then, using equation (1) and the measured dose rate, the age of the event in question can be approximated. Although OSL dating is only useful in certain situations, it provides an

excellent way of determining the age of specific events, and is capable of doing so for dates from 0.01 ka and up to >100 ka in ideal situations (Rink, 2001; Schwarcz, 2002). Optically stimulated luminescence dating of quartz grains has become the most commonly used method of luminescence dating due to its reliability and applicability in a diversity of situations (Duller, 2008).

3.1.2. Electron Trapping

OSL is based on the accumulation of electrons at vacant or defective atomic sites throughout the volume of a crystal lattice (Rink, 2001). These sites are broadly distributed within a crystal, as they are either related to impurities which were included throughout during crystallization, or disruptions in the crystal lattice such as atomic scale structural defects. Since these defect sites are only somewhat different from the rest of the lattice, the charge states associated with them are also a little different (Rink, 2001). In luminescence dating, these metastable states are called 'traps'. The simplest way of understanding how these charge traps work is with the energy band theory of solids, which divides energy levels of electrons in a lattice into three main parts: the valence band, the conduction band, and the forbidden zone (Feathers, 1997). The valence band represents the ground state of electrons which are found in the chemical bonds of the crystal lattice, while the conduction band represents an excited state of electrons which have been energized by radiation. The forbidden zone is the region between the valence band and the conduction band and denotes the energy levels at which electrons should not be stable in a given crystal lattice. However, the existence of defect sites mentioned previously creates 'traps' in the forbidden zone, which cause some excited electrons to become captured in a metastable state (Rink, 2001). This process of trapping is explained in Figure 2 below.

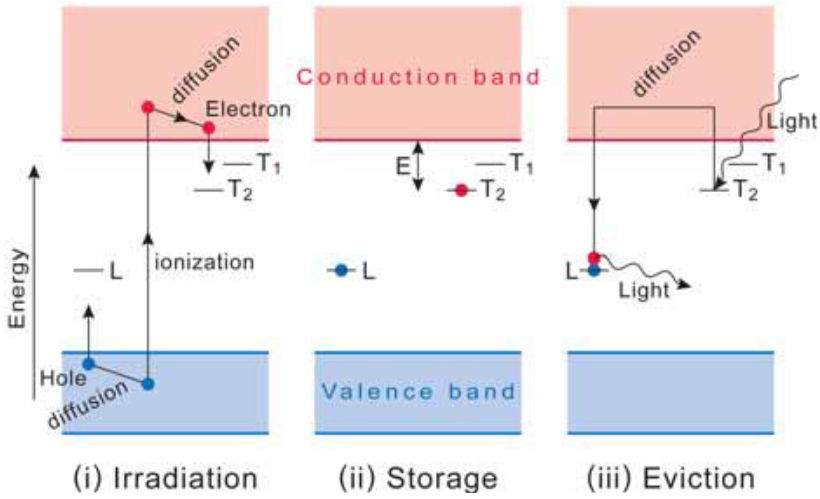

Figure 2. This diagram shows how the energy band theory relates to the process of luminescence.
(i) Irradiation of crystal induces ionization, sending electrons into the conduction band.
(ii) Excited electrons are trapped at defect sites, where they are stored for a length of time which correlates with the "depth' of the trap (E). In this case, T_2 is deeper than T_1, so an electron trapped in T_2 is more stable than one trapped in T_1, which means that it will remain trapped in T_2 for a much longer period of time without stimulation.
(iii) Exposure to light or heat stimulates the crystal and ejects trapped electrons, allowing them to recombine with holes at luminescence centres (L). This process releases the stored energy as photons and it is these photons that make up the luminescence signal.
Figure and text adapted from Duller (2008).

Throughout an extensive period of time, if a crystal is shielded from bleaching sources (usually by burial or inclusion in another material), it continuously accumulates charge at defect sites due to this process of electron excitement and trapping (Rink, 2001). Incoming radiation from the natural environment transfers energy to a crystal via ionization of atoms in the lattice, leading to the notion of trapping electrons at sites such that their energy states are higher than normal. This radiation can be in the form of alpha, beta, gamma and cosmic rays (Feathers, 1997). When the crystal is stimulated by exposure to light or heat, the trapped electrons are released with retained energy, resulting in the phenomenon of luminescence (Duller, 2008). After all of the charge traps have been emptied from a mineral grain, it is once again bleached, a state that can be achieved in less than ten minutes of exposure to direct sunlight (Schwarcz, 2002).

3.1.3. Importance of Trap Depth

The term trap depth is used to describe the amount of energy that is needed to release charge from a trap (Feathers, 1997). Traps get 'deeper' when they reside farther from the valence and conduction bands. This means that more energy is required to eject electrons, so deep traps are more stable than shallow ones. For example, in Figure 2, T_1 represents a shallow trap with an average lifetime of 20 hours, while T_2 represents a deeper trap which is stable for millions of years (Duller, 2008). Although the shallow trap

is useless, the deeper trap is very useful for dating as it covers a large timeframe and its stability has been confirmed by its use in the dating of sediments nearly a million years old (Duller, 2008). This is the trap that is used in OSL dating of quartz grains. In order to isolate the luminescence signal from this trap, the signal from shallower traps must be zeroed after artificial irradiation in laboratory (Schwarcz, 2002). This is done by preheating the sample to eject any electrons residing in any of the shallow traps. The temperature of the preheat is selected based on the amount of energy needed to empty the shallow traps while leaving the deeper trap of interest unaffected after a known dose, and usually lies between 160°C and 300°C (Duller, 2008). Charges trapped in the second, more stable trap can be released by exposure to visible light (Schwarcz, 2002; Duller, 2008). Once electrons are released from a trap by excitation by visible light, they can then recombine with holes at luminescence centres. As this occurs, the surplus energy is emitted in the form of photons which make up the luminescence signal (Feathers, 2003).

3.2. Laboratory measurement of Optically Stimulated Luminescence (OSL)

In the laboratory measurement of optically stimulated luminescence (OSL), mineral grains are irradiated with light of a certain wavelength that can be filtered and which liberates the trapped charges, resulting in the emission of light of a shorter wavelength that can be detected (Schwarcz, 2002). The mineral grains luminesce as soon as the light begins to stimulate them; hence the term optically stimulated luminescence. The luminescence signal from quartz is initially bright, then decays exponentially as charges are vacated from their traps (Duller, 2008). The initial rapid decay, referred to as the dominant fast component, occurs as luminescence is emitted from the traps which are most easily bleached. The following slower decay (medium and slow components) then appears as luminescence is emitted from traps which are less easily bleached (Aitken, 1998). Complications such as various retrapping mechanisms or the presence of different kinds of traps with differing energies can affect the form of the luminescence signal since charges have an altered reaction to stimulation, but fortunately this was not observed in the samples studied here (Feathers, 1997).

The light used for stimulation must be limited to a small range of wavelengths that is significantly discernible from the emission wavelength of the mineral (Figure 3) such that it can be completely filtered so that the detector only senses light from the luminescence signal (Schwarcz, 2002; Duller, 2008). Blue light emitting diodes (LEDs) are generally used to stimulate mineral grains, as the light can be easily filtered and causes both quartz and feldspar to produce an OSL signal (Duller, 2008). The peak emission of OSL in quartz lies between 365-380 nm (near-UV), while the emission of the blue LEDs (light emitting diodes) used for stimulation is centered near 470 nm. In order to ensure that none of the light from the stimulation source is detected, the photomultiplier tube (PMT) is protected by a filter which is opaque to blue light, but still allows UV light produced by the stimulation of quartz to pass through into the detection window. A Hoya-U340 filter is typically used when blue LEDs are being employed for stimulations (Rhodes, 2011).

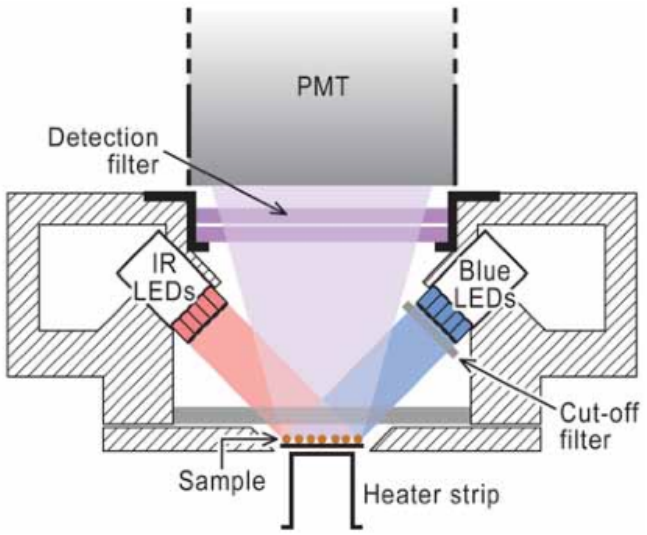

Figure 3. A schematic of the standard Risø OSL unit containing blue (470 nm) and IR (875 nm) LEDs (Bøtter-Jenson et al., 2010).

Infrared LED's have a peak emission centered around 875 nm, and can also be used to stimulate mineral grains. This type of luminescence is called infrared stimulated luminescence (IRSL), and is most commonly detected from feldspars. At room temperature, quartz does not emit an IRSL signal. This fact can be exploited to check the purity of a quartz sample relative to feldspar contamination for OSL measurements.

3.3. Single-aliquot regenerative dose (SAR) protocol

Equivalent dose measurements can be accomplished using either the additive dose method or the regeneration approach, the latter of which is now more frequently used (Duller, 2008). This study employed the single aliquot regeneration (SAR) approach, which uses a series of measurements and regeneration doses to calibrate the luminescence signal of each sample (Murray and Wintle, 2000). The SAR protocol is comprised of a series of repeated steps that are delineated in Table 3. The first step is to measure the unknown natural OSL signal (L_N), which represents the luminescence signal generated by the radiation that the sample was exposed to in nature since the last bleaching event. Next, a test dose, which is a small known dose of laboratory radiation, is applied, and following a cut-heat, the OSL signal is measured. Samples are then repeatedly bleached and irradiated with varying known regeneration doses (including a 0 Gy dose and repeat dose cycle) and, after a preheat, the resulting luminescence signals are measured (during stimulation by blue LEDs for 100s at 125°C) (Meidahl and Christiansen, 1994). These regenerative dose responses are used to create curves which describe the development of

a luminescence signal after bleaching in relation to exposure by unit dose. These curves are then used to determine the amount of laboratory dose (equivalent dose) that was required to obtain a luminescence signal that replicates the natural signal (paleodose) (Duller, 2008).

Every OSL measurement is preceded by a preheat, the purpose of which is to remove any unstable electrons from shallow traps. The heating prior to the test dose referred to as the cut heat, is usually done at a temperature similar to or lower than the preheat. After each test dose is measured, an illumination step is performed at high temperature to evacuate any remaining trapped charge prior to the next measurement cycle (Murray and Wintle, 2000, 2003) (Table 3).

It is accepted that the luminescence sensitivity of a given aliquot (a small portion of a sample mounted on an aluminum disc) changes during a SAR measurement sequence. In order to deal with this complication, it is essential that for each OSL measurement taken, the sensitivity change is also quantified. This is achieved by giving a specific dose, known as a test dose, after every OSL measurement, then recording the new test dose response (T_i). Changes in sensitivity can then be discerned by a comparison of the measurements of the natural and regenerative-dose responses to the ensuant sensitivity (L_x/T_x). These points plot as a growth, or dose-response curve, which is fitted with a single saturating function. The D_E is determined by finding the intercept of the natural luminescence signal with the growth curve (Murray and Wintle, 2000, 2003).

Table 3. A typical SAR sequence used for quartz OSL measurements (Murray and Wintle, 2000)

Step	Treatment	Observed
1	Natural or given dose, D_i	--
2	Preheat (160-300 °C for 10 s)	--
3	Stimulate for 40 s at 125 °C	L_i
4	Give test dose, D_t	--
5	Cut heat (160-300 °C)	--
6	Stimulate for 40 s at 125 °C	T_i
7	Stimulate for 40 s at 280 °C	--
8	Return to step 1	--

A major benefit of using the SAR protocol is that it contains several built-in checks which are used to evaluate the luminescence behaviour of each aliquot. The recycling test is used to judge the ability of the SAR protocol to account for sensitivity changes. This test compares the final regeneration dose response to the first regeneration dose response of equal magnitude. The ratio between these two sensitivity-corrected luminescence signals is called the recycling ratio, and if it is equal to 1, the implication is that the SAR protocol was able to effectively correct for sensitivity changes which came

about throughout the measurement process. Acceptable values for the recycling ratio lie within 10% of 1 (0.9 to 1.1), if the ratio is greater or less than this, it is likely that the SAR protocol was unable to effectively account for changes in sensitivity and therefore may not be suitable for the measurement of those samples.

The SAR protocol also includes a recuperation test, which is performed by the inclusion of a zero dose in the sequence of regenerative doses. In theory, the sensitivity corrected signal (L_0/T_0) resulting from a zero dose should be near zero. Any value above this suggests that there is some signal retention, possibly induced by the preheating of the sample prior to measurement as a result of thermal transfer. Pragmatically, it is not unusual to observe a small signal, but this is deemed insignificant if the value is less than 5% of the natural signal (L_N/T_N).

CHAPTER 4: METHODS

4.1 Sample Collection & Preparation

A total of 11 sediment samples were collected during June 2013 on the Tyndall Air Force peninsula (N 29.96838, W 85.45601; approximately 5 m ASL) in two separate excavation units: EU5 and EU6 (Figure 4). EU5 is believed to represent the 8By31 mound, with EU6 located approximately 25 m to the southwest representing part of the large Hare Hammock ring. All samples were collected at 10 cm intervals down the profile to a depth of 60 cm. Prior to sample collection, the exposed profile walls were cut back vertically to remove the exposure and exclude the sampling of loose, light-exposed material. Samples were collected in copper tubes which were inserted horizontally into the vertical profile. Once filled with sediment, the tubes were cautiously removed from the profile and packed tightly with aluminum foil stoppers on either end to prevent the sediment from shifting or mixing. They were then sealed with opaque black tape on either end and wrapped in aluminum foil to ensure the samples remain protected from exposure to light.

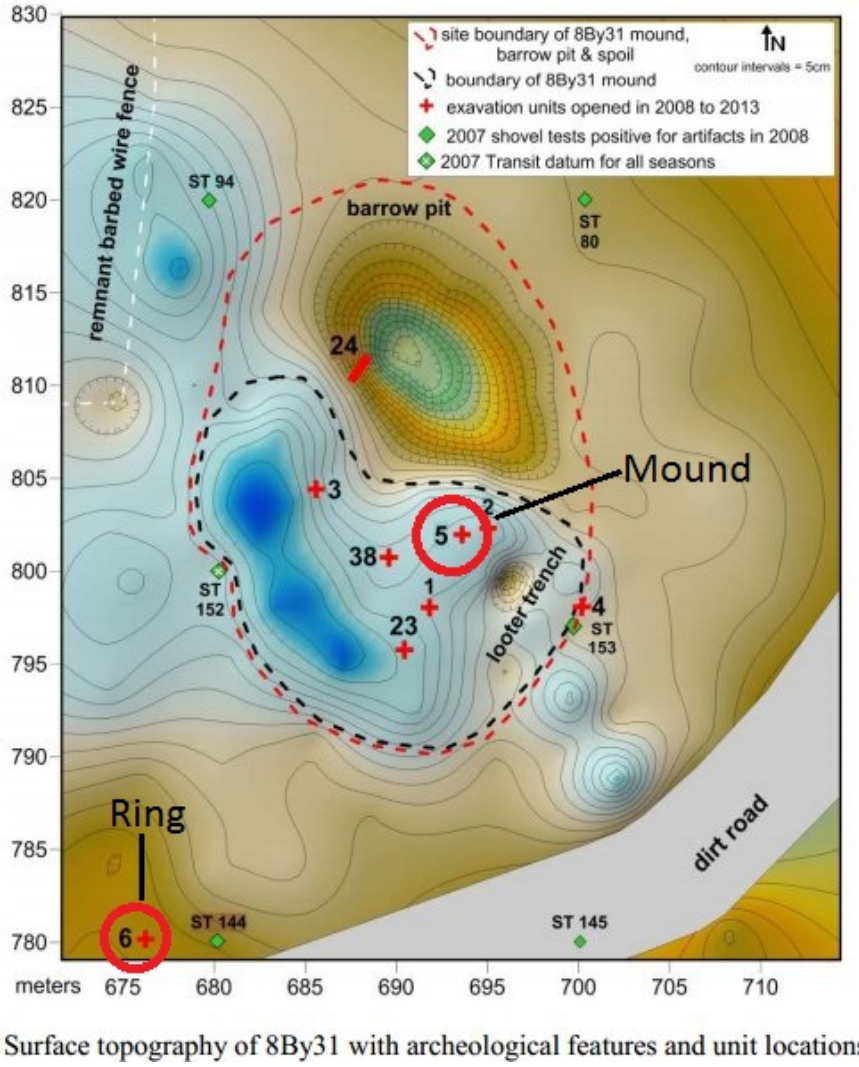

Figure 4. Schematic showing the locations of excavation units, with EU5 located near the center of the image and EU6 located at the bottom-left.

All samples for OSL were transported to the *AGE Laboratory* at *McMaster University* in sealed tubes to preserve both the moisture content and the luminescence signal (Lopez, 2007). Samples were weighed immediately after being opened, and then oven dried *(~60 °C)* and reweighed to obtain the moisture content. This moisture content was assumed to be the best representative of past conditions. A small portion of the whole sediment from each sample *(~1 g)* was then taken for Neutron Activation Analysis (NAA) and Delayed Neutron Counting (DNC) to obtain elemental concentrations used for dosimetry measurements (Lopez and Rink, 2007). Samples were then treated with 10%

HCl to dissolve carbonates and rinsed. It is imperative that all $CaCO_3$ is completely removed from the samples to ensure that no CaF_2 is formed when they are later treated with HF (Meidahl and Christiansen, 1994). Any organic material present was then removed using 30% H_2O_2 (Lopez, 2007). After the initial chemical treatments, samples were rinsed, dried and sieved and a suitable grain size distribution was selected to use for dating. The 90-150 μm grain size fraction was used for the dating of all samples in this study. A heavy liquid solution of lithium polytungstate prepared to have a specific density was then used to perform mineral separations. Heavy minerals such as illmenite and zircon were separated using a liquid with a density of 2.75 g/ml (Meidahl and Christiansen, 1994). This leaves only the quartz and feldspars, which cannot be separated using heavy liquids because they have overlapping densities. A pure quartz sample was obtained by dissolving the feldspars using 40% HF for 40 minutes (Lopez, 2007). Samples were then rinsed, treated one last time with 10% HCl for 15 minutes to remove any fluorides that may have formed during the previous treatment, then rinsed again and dried. The purity of the quartz was confirmed after treatment for all samples by verifying that they produced no significant signal when exposed to infrared light (Meidahl and Christiansen, 1994). All sample preparation and dating was performed in a darkroom under dim, UV-filtered orange light to prevent any bleaching by exposure to natural light.

4.2 Dosimetry

Dosimetry was performed for this project using the following two techniques described here:

1) Aluminum oxide dosimeters (Al_2O_3:C)

Highly radiation-sensitive Al_2O_3:C crystal cylinders were used for this study as dosimeters to perform *in-situ* dosimetry based on the method developed by Kalchgruber and Wagner (2006). This technique uses a pair of dosimeters in each sample location to measure both beta and gamma dose rates separately and simultaneously. The separate measurements are accomplished by differential shielding of the two dosimeters. One of the dosimeters in each pair is put in a stainless steel casing which shields it from beta radiation, thus it records only gamma and cosmic doses. The other dosimeter is wrapped only in electrical tape to protect it from light, so it records beta, gamma and cosmic doses. The beta dose rate can be isolated by calculating the difference in total dose received by a given pair of dosimeters, and the gamma dose rate can be calculated by removing the modelled present cosmic dose from the value reported by the Al_2O_3:C chip in the stainless steel casing.

These dosimeter pairs were attached to the end of wood dowels so they could be inserted into the OSL sampling locations. The Al_2O_3:C dosimeters were set at the back of the hole from which the sediment was extracted, where they remained buried for 341 days to accumulate the environmental dose. They were then excavated and sent to North Carolina University for dose measurement performed by Dr. Regina DeWitt.

All dosimeters were transported along with 8 travel dosimeters which were zeroed before transport, and evenly distributed around in order to accurately record the dose accumulated during transportation and storage in the lab before measurement. The thermoluminescence (TL) signal from these dosimeters was measured using a Risø TL-DA-15 with a Hoya U-340 filter and heating up to 400 °C at a rate of 5 °C/s. The signal was integrated under the primary dosimetric peak appearing at around 200 °C. A 5 s given dose was also applied to obtain a signal which was used to calibrate for different sensitivities between Al_2O_3:C cylinders.

A separate set of dosimeters used for calibration were buried for 159 days in a reference soil which has a well-known dose-rate (Nussi, Antoine et al. 2001; Kalchgruber and Wagner, 2006). However, the volume of sediment was not enough to achieve full 4π geometry, so an alternate approach was used to calibrate the gamma dose. A ^{60}Co gamma source was used at the Nuclear Reactor Program at North Carolina State University to irradiate the Al_2O_3:C chips encased in steel, and the absorbed gamma and cosmic dose was measured using the same Risø machine which was calibrated against these dosimeters, fitted with a ^{90}Sr beta source.

Dose measurements were made using the travel-corrected signals acquired from the travel dosimeters. For the steel encased dosimeters, this provides the combined gamma and cosmic dose absorbed during 341 days of burial, which was converted to an annual dose. The calculated modern cosmic dose rate can then be subtracted from this value to obtain the gamma dose alone.

Since the Al_2O_3:C chips not encased in steel also attenuated beta radiation, they had to be treated differently. The reader was calibrated using the dosimeters buried in the Nussi reference material for a mixed beta-gamma field, in which gamma radiation completely penetrates the cylinders while beta radiation is attenuated. By using this calibration, the combined beta + gamma + cosmic dose was measured. The gamma and cosmic dose (determined from the steel encased dosimeter) was subtracted from this to acquire just the beta dose.

2) Neutron activation analysis (NAA) and Delayed Neutron Counting (DNC)

Prior to any treatments, small subsamples were taken from the original samples and used to determine the elemental concentrations of radioactive isotopes present. This was achieved using neutron activation analysis (NAA) of ^{232}Th, ^{40}K and delayed neutron counting (DNC) analysis of ^{238}U, all conducted by the Centre for Neutron Activation Analysis (NAA) at the McMaster University Nuclear Reactor. Both methods were performed using the "comparator" approach, which is considered one of the most accurate methods of quantifying elemental concentrations. Samples were irradiated together with standards containing known amounts of the elements. After irradiation, both samples and standards were

measured with the same detector under identical conditions (Alice E. Pidruczny, Laboratory Services Manager, Centre for NAA, McMaster Nuclear Reactor). This procedure eliminates uncertainties in the nuclear parameters and detector efficiencies, greatly reducing measurement uncertainties. Errors for each of the elemental concentrations were determined based on the standard deviation of the detected gross counts and background counts, added in quadrature. Based on these concentrations, environmental dose rates were calculated using ANATOL software. Energy release tables of Guerin et al. (2011) were used to determine dose rates.

4.3 Luminescence Measurements

OSL measurements for this project were taken using a Risø TL-DA-15 luminescence reader equipped with a 6 mm-thick Hoya U-340 UV transmitting filter. An attached $^{90}Sr/^{90}Y$ (beta) radioactive source was used to perform laboratory irradiations. The determination of a sample's final equivalent dose was accomplished using the following three step process:

1) **Initial D_E & feldspar contamination check**
   An estimation of the initial D_E was made by comparing the natural OSL signal of four aliquots per sample to their OSL signal after a given dose. The same regenerative dose was repeated on each aliquot and the resulting IRSL signal was recorded. Infrared stimulated luminescence measurements were taken at 125ºC for 100s under IR diodes. For all samples, the ratio of IRSL after dose to OSL after dose was <0.005, therefore no significant feldspar contamination is present. The range of initial D_E's observed were used to determine the selection of regenerative doses required to determine the final D_E of each sample.
2) **Dose recovery test**
   Dose recovery tests were conducted on all samples to ascertain the most appropriate preheat temperature for recovering a given dose using the SAR protocol. This data was obtained using preheat temperatures of 160ºC, 200ºC, 240ºC, and 280ºC, for 10s each and bleaching conditions of 125ºC under blue LEDs for 100s. At each preheat temperature, three aliquots were measured, requiring a sum of twelve aliquots per sample. The preheat temperature that provided a dose proximal (within error) to the given dose was chosen for use in the final D_E measurement.
3) **Final D_E measurement**
   OSL measurements for the estimation of final equivalent doses were collected on 48 aliquots for each sample using a 0.5 mm mask size. The SAR protocol was followed for all measurements. The OSL signal was integrated from channels 1 to 2 (the first 0.4 s of emission), and the subtracted background was integrated from the final 10 channels (the last 4 s) of the OSL decay curve.

A generalized overview of the treatment steps which comprise the SAR protocol is as follows:

Step	Treatment
1	Natural or Given dose, D_i
2	Preheat (200 °C for 10 s)
3	Stimulate for 40 s at 125 °C
4	Give test dose, D_t
5	Cut heat (160-300 °C)
6	Stimulate for 40 s at 125 °C
7	Return to step 1

A sensitivity-corrected dose-response curve was generated from the sensitivity-corrected regenerative-dose points (L_X/T_X) recorded, to which a saturating exponential function was fitted. The corresponding sensitivity-corrected natural signal (L_N/T_N) was then interpolated from each dose-response curve to obtain a D_E estimate.

Aliquots were rejected on the basis of the following statistical criteria:

Criteria	Limit
Recycling ratio	> 10%
Recuperation	> 5%
Signal to background noise ratio	< 3:1
Test dose error	> 5%
Paleodose error	> 5%

Figure 5 shows an example of an OSL decay curve and a dose response curve for an aliquot from the sample EU5-2**,** which is representative of all collected data and demonstrates the good OSL behaviour of quartz from this region.

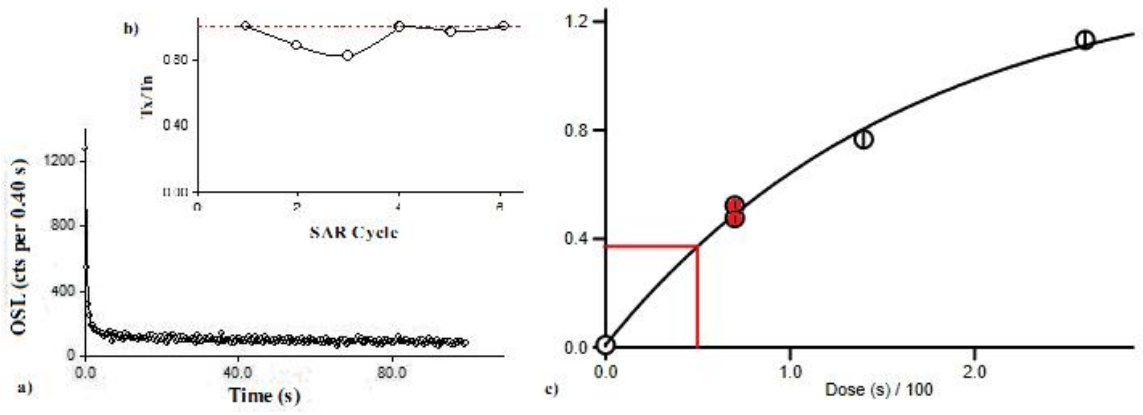

Figure 5. a) Example OSL decay curve from the sample EU5-2; b) Tx/Tn graph showing sensitivity changes throughout the SAR protocol for the same aliquot; c) Dose response curve produced for this aliquot, with red-filled circles representing the repeated given dose.

4.4 Equivalent dose determination

The primary goal of luminescence dating is to determine the amount of radiation which would be required to cause a material to accumulate the present charge population (Rink, 2001). In other words, the paleodose, or equivalent dose (D_E) is a measure of the total radiation that a mineral would have to be exposed to in order to produce the observed luminescence signal (Schwarcz, 2002). The amount of light emitted by a sample varies from grain to grain depending on their unique geological histories (Duller, 2008). As such, measurements must be performed on a number aliquots of a sample to obtain an overall estimation of the equivalent dose.

The equivalent doses measured for accepted aliquots from each sample were plotted using both a probability density function and radial plots. There are two different models used to determine equivalent dose estimates from the D_E distributions observed from the measured aliquots of each individual sample. These are the central age model (CAM), which calculates the central dose equivalent to the geometric mean of the distribution of measured palaeodoses, and a minmum age model (MAM), which isolates populations of younger grains by applying a truncated normal distribution (Galbraith et al. 1999; Galbraith and Roberts, 2012). The minimum age model is usually favoured when dating sediments which have either been only partially bleached or mixed with older sediment by some form of post-depositional disturbance (or both).

In order to determine the most appropriate age model to apply, skewness and kurtosis were calculated for all samples in RStudio using the dbED function in the numOSL package by written by Peng Jun, which also provides an age model

recommendation based on these values, using the criteria described in Bailey and Arnold (2006). Central and minimum doses were also calculated in RStudio, using functions provided in the Luminescence package written by Christoph Burow (University of Cologne, Germany), based on a rewritten S script by Rex Galbraith, 2010. For the samples in this study, the 3-parameter minimum age model (MAM-3) (after Galbraith et al., 1999) was recommended almost unanimously, with the exception of one sample (EU5-3). These isolated equivalent dose estimates were then used for final age calculations.

A σ_b value was also determined by using aliquot diameter, grain size, and a 3% machine error (after Cunnigham et al., 2011), then added in quadrature to all D_E estimates. This accounts for the variations resulting from both instrumental error and intrinsic luminescent properties (Galbraith et al., 2005). For more details see footnotes in Table 4.

4.5 Age Determination

Ages were calculated by dividing the equivalent dose over the calculated annual dose rate (d) (determined by either chemical analysis or Al_2O_3:C dosimetry) to obtain an age (t), using this equation:

$$t = D_E / d \qquad (1)$$

All ages, error estimates, and dose rate calculations were computed using ANATOL v. 2.0.52 software (Mercier, 2012), which includes the dose rate conversion factors published by Guérin et al. (2011). External beta dose rates were calculated using the concentrations of ^{238}U, ^{232}Th and K in the sediment (measured using neutron activation analysis (NAA) and delayed neutron counting (DNC)) assuming secular equilibrium in the ^{238}U and ^{232}Th decay chains. The gamma doses reported by in-situ Al_2O_3:C dosimetry were used as the external gamma dose rates to calculate the ages for 10 of the 11 samples dated. The sample EU6-6 had a dosimeter in place which was never recovered, so the environmental dose rates (gamma and beta) were calculated based purely on the elemental concentrations determined by NAA and DNC. A correction for attenuation in water was applied to all beta and gamma dose rates based on the estimated moisture content during measurement (Mejdahl & Christiansen 1994), which is assumed to have been relatively constant through history. The external alpha dose is rendered insignificant by the removal of the outer, alpha-exposed layer as the quartz grains are etched during the 40% hydrofluoric acid treatment, and is therefore irrelevant to the environmental dose rate calculation.

Cosmic radiation doses for all samples were based on latitude and the thickness of the overlying sediment, which provides shielding (as per Prescott and Hutton 1994). These were calculated in R using an overburden density of 2 g/cm^3 and the cosmic dose

rate data from Adamiec and Aitken (1998). Both of the stratigraphic sections analyzed are assumed to have been deposited rapidly over a period that was short in comparison to their total age, thus the currently measured sample depths were used for this calculation (instant accumulation model). Internal dose was calculated using the elemental concentrations of ^{238}U (0.06650 ± 0.02194 ppm) and ^{232}Th (0.11350 ± 0.04248 ppm) measured from granitic quartz by Rink and Odom (1991). Absorbed beta fractions follow from the work of Mejdahl (1979). Uncertainties in the final age calculations were based on a combination of the errors on the annual and equivalent doses, as well as the following systematic errors: a) ± 25% for moisture content; b) ± 2% for etching; c) ± 10% for cosmic dose rate, and d) ± 10% global systematic error.

CHAPTER 5: RESULTS

5.1 Luminescence behaviour

A dose recovery test was conducted on all samples to assess the effects of varying preheat temperatures on the resulting D_E value. For all samples studied, the equivalent dose (D_E) seems to be relatively unaffected by preheat temperatures within the range of 160 °C and 280 °C, but overall displays best accordance when given doses are performed at 200 °C. Preheat temperature also appears to be inconsequential to the value of recycling ratios and recuperation. Figure 5a shows an example of an OSL decay curve and a dose response curve for an aliquot from the sample EU 5-2, which is representative of all collected data and attests to the good OSL behaviour of quartz collected from this site. The OSL signal decayed rapidly in all samples, intimating a dominant fast component to the signal. Luminescence properties are generally consistent throughout both of the profiles studied. All dose response curves can be closely delineated by a single saturating exponential function, with natural signals well below the level of laboratory saturation. Figure 5b also depicts the overall behaviour of the sample during the SAR protocol. The repeatability of measurements of points on the dose response curve is a testimony to the accuracy of the corrections made for sensitivity changes induced by the repeated irradiation and bleaching cycles (Figure 5c, red-filled circles).

5.2 Equivalent Doses

The equivalent dose distributions obtained for all measured samples are displayed graphically as probability density plots and radial plots in Figures 6 and 7. A variety of statistical attributes for these D_E distributions are listed in Table 4. Using 0.5 mm multi-grain aliquots, overdispersion values range from 17% to 63% in the EU6 profile and from 25% to 77% in the EU5 profile. Dose distributions appear to be positively skewed with overdispersion values notably larger than would be anticipated from intrinsic sources of variability, based on the results of dose recovery tests. It is common for near surface

samples to have relatively high overdispersion values, as demonstrated by EU5-1, EU5-2, and EU6-1. Although the results generally exhibit significant scatter, very few display evidence of multi-modal distributions. Kurtosis values vary widely, but are generally higher in samples for which a greater number of aliquots were accepted, thus creating a more distinctive peak in the data. The fraction of accepted aliquots appears to be greater in samples from EU6 than EU5. Based on these statistical data, it was determined that the 3-parameter minimum age model (MAM-3) is the most appropriate method to evaluate equivalent doses for all samples, with the exception of EU5-3, for which the central age model (CAM) was selected.

Table 4. Summary of statistical data for samples in EU5 and EU6 at Hare Hammock

Sample	Depth (cm)	Aliquot Diameter (mm)	Grain Size (μm)	σ_b [a]	# of Accepted Aliquots	OD [b]	c [b]	k [b]	Suggested Model
EU6									
EU 6-1	10	0.5	150 - 212	14.4%	22/48	62%	2.44 ± 0.52	4.86 ± 1.04	MAM3
EU 6-2	20	0.5	150 - 212	14.4%	29/48	17%	0.97 ± 0.45	0.58 ± 0.91	MAM3
EU 6-3	30	0.5	150 - 212	14.4%	25/48	32%	1.65 ± 0.49	3.39 ± 0.98	MAM3
EU 6-4	40	0.5	150 - 212	14.4%	38/48	49%	5.77 ± 0.40	21.67 ± 0.79	MAM3
EU 6-5	50	0.5	150 - 212	14.4%	31/48	63%	3.07 ± 0.44	12.6 ± 0.88	MAM3
EU 6-6	60	0.5	150 - 212	14.4%	24/48	58%	1.03 ± 0.50	0.7 ± 1.0	MAM3
EU5									
EU 5-1	10	0.5	150 - 212	14.4%	5/48	74%	0.14 ± 1.1	-2.64 ± 2.19	MAM3
EU 5-2	20	0.5	150 - 212	14.4%	10/48	77%	1.91 ± 0.77	1.73 ± 1.55	MAM3
EU 5-3	30	0.5	150 - 212	14.4%	7/48	25%	0.23 ± 0.93	-0.16 ± 1.85	CAM
EU 5-4	40	0.5	150 - 212	14.4%	12/48	33%	1.20 ± 0.71	1.13 ± 1.41	MAM3
EU 5-5	50	0.5	150 - 212	14.4%	24/48	29%	1.51 ± 0.50	3.95 ± 1.0	MAM3

Table Footnotes:
[a] σ_b value determined using aliquot diameter, grain size, and a 3% machine error (after Cunnigham et al., 2011).
[b] These values were calculated in RStudio using the dbED function in the numOSL package by Peng Jun, based on the model presented in Bailey and Arnold (2006), which also provides criteria for determining the most statistically favourable age model to apply to the data, presented in the final column.

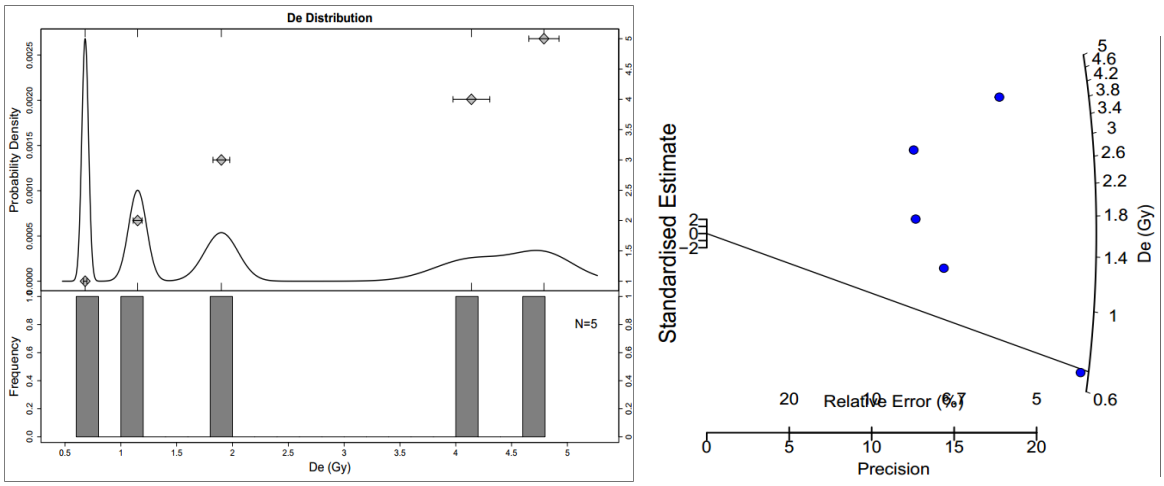

EU5-1

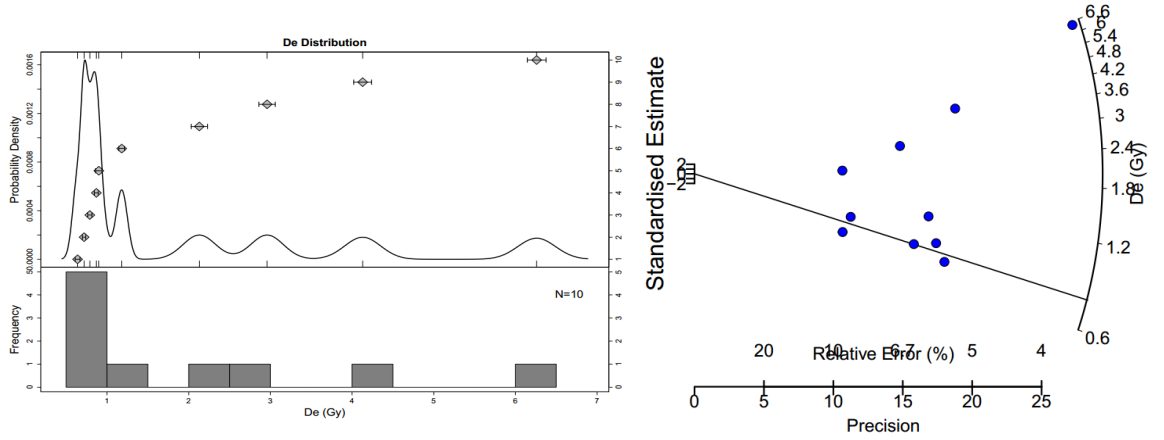

EU5-2

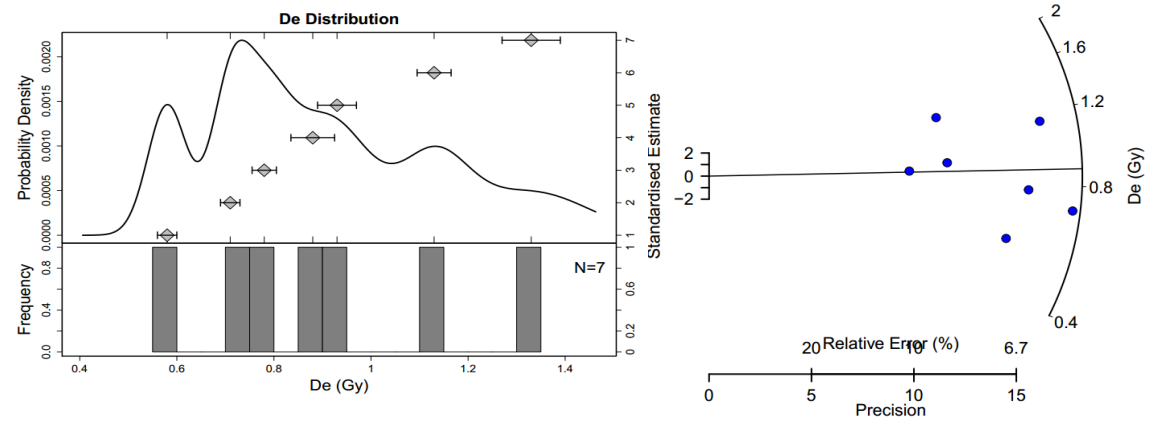

EU5-3

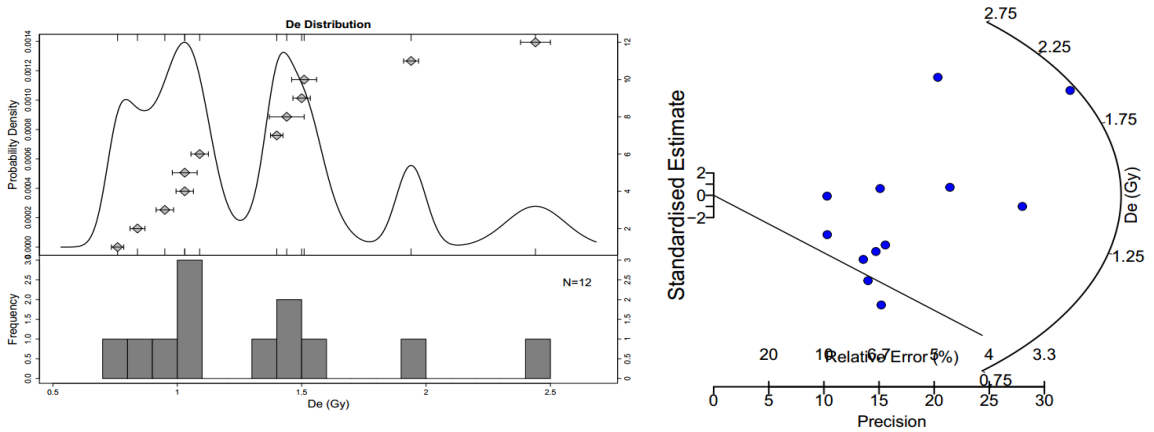

EU5-4

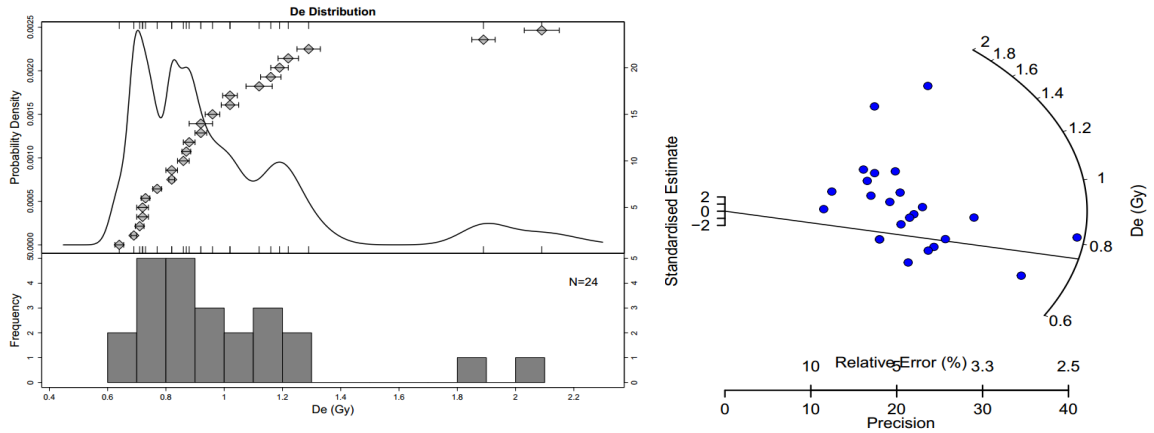

EU5-5

Figure 6. Probability plots and radial plots for the EU5 profile

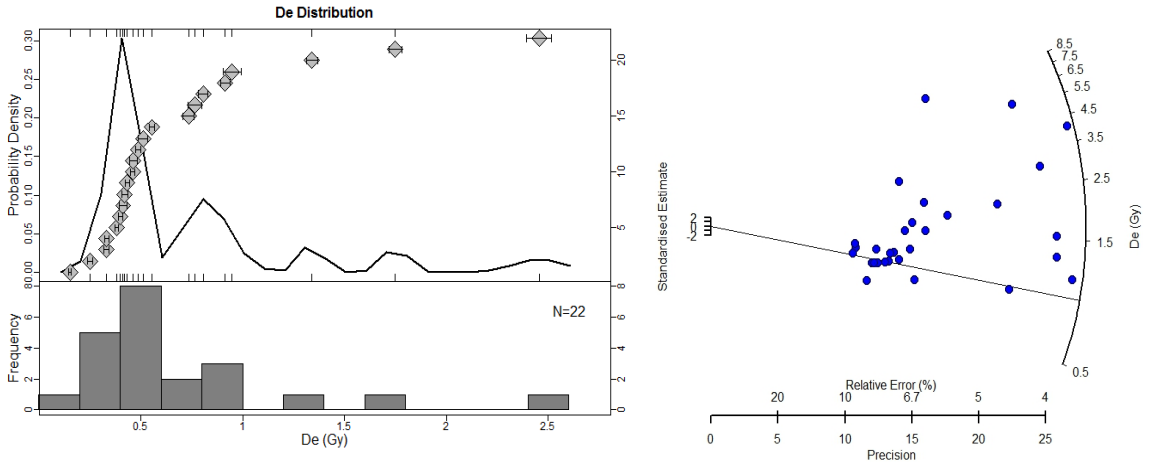

EU6-1

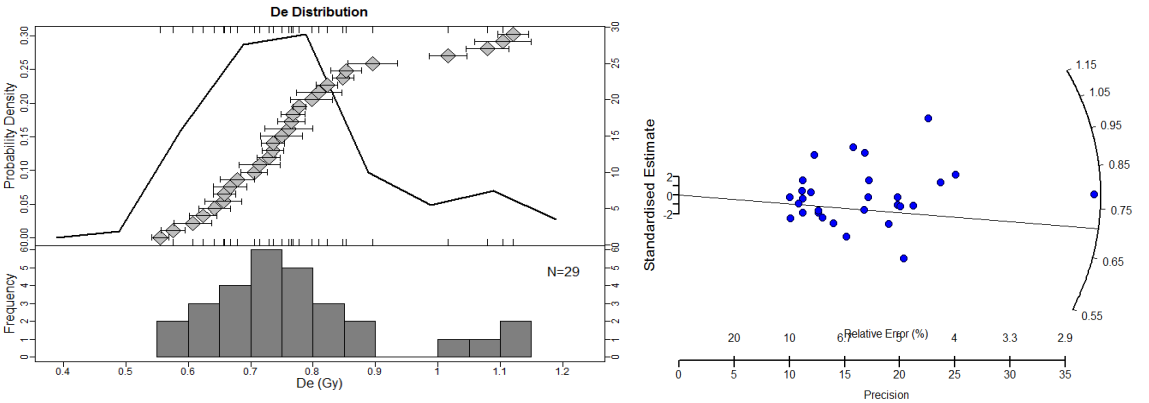

EU6-2

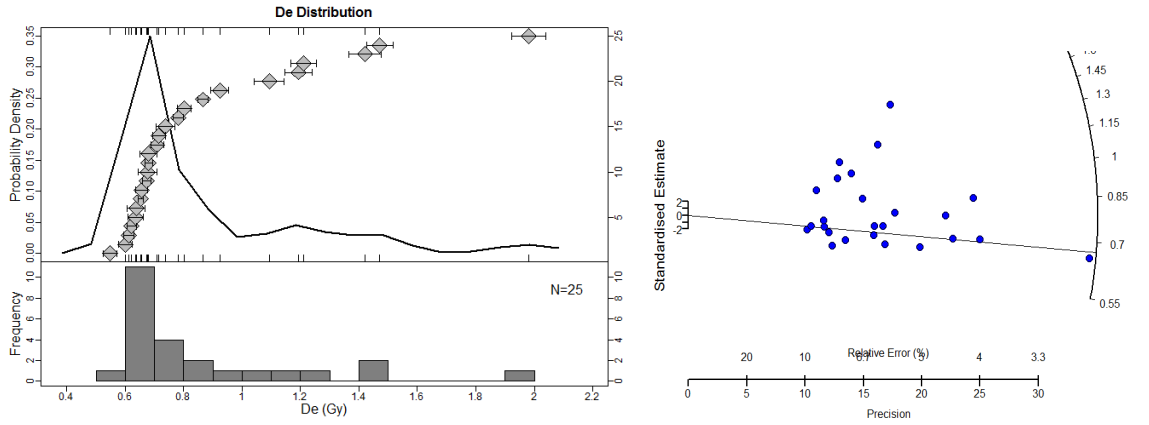

EU6-3

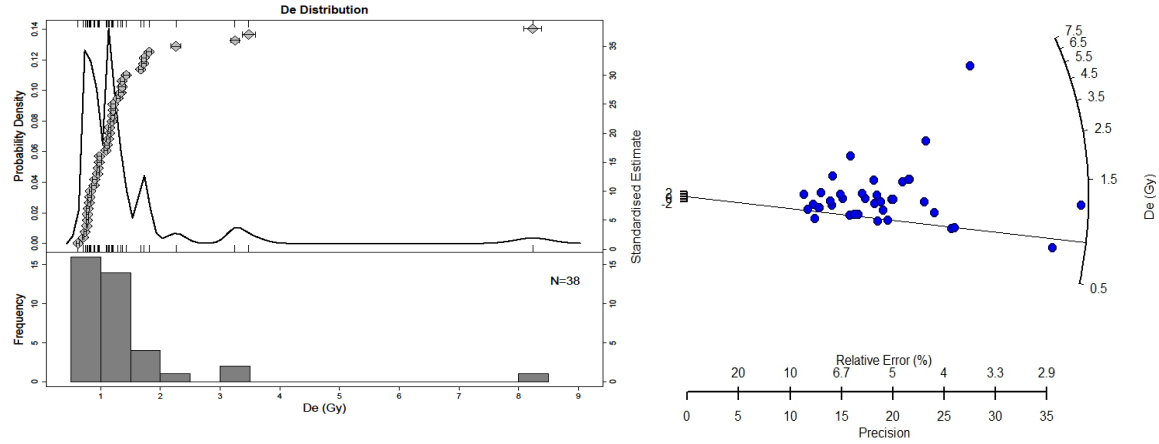

EU6-4

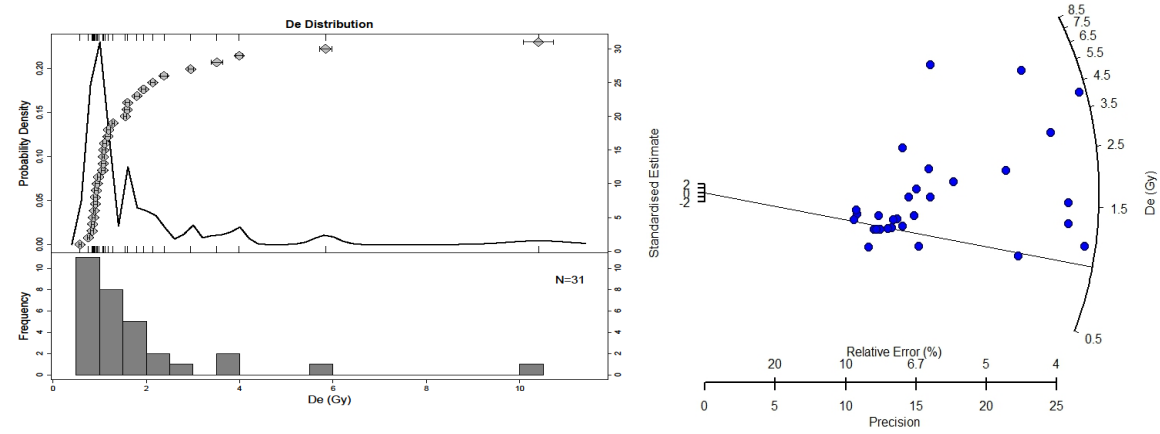

EU6-5

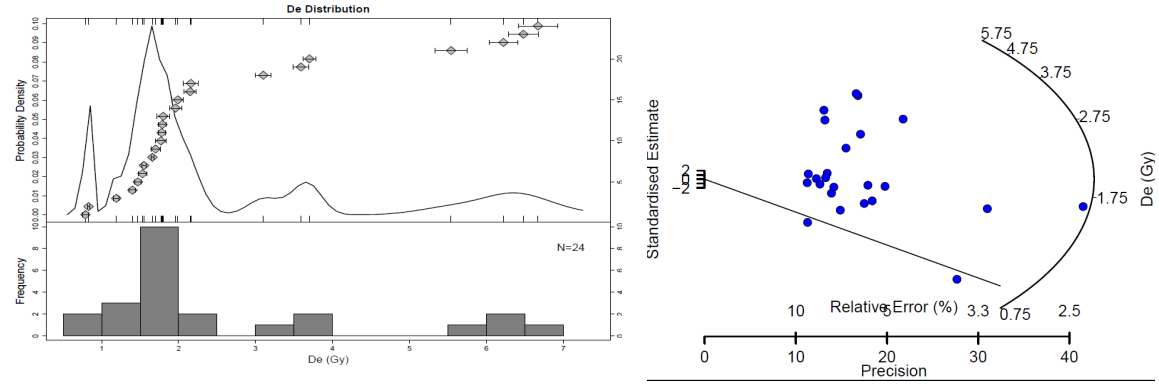

EU6-6

Figure 7. Probability plots and radial plots for the EU6 profile

5.3 Dosimetry

5.3.1 NAA/DNC Dose Rates

Radionuclide concentrations determined by neutron activation analysis (NAA) and delayed neutron counting (DNC) are presented in Table 5. Samples from EU5 generally have higher concentrations of ^{238}U and ^{232}Th than samples from EU6. K content, on the other hand, is actually higher in most of the samples from EU6 than EU5, especially the two uppermost samples from 10-20cm below the surface. Figure 8 depicts the changes in the concentrations of these radionuclides with depth in each profile sampled. Changes in ^{238}U and ^{232}Th concentrations are coincident but not always equal, while changes in K seem to be independent. ^{232}Th concentrations are always higher than that of ^{238}U and the associated variation exhibited is often more exaggerated. Both have spikes at -20cm and -60cm in EU6 and at -10cm and -40cm in EU5. The two profiles appear to be the inverse of one another, with a particularity strong ^{232}Th spike occurring at the top (-10cm) of EU5 and at the bottom of EU6 (-60cm). K concentration in EU6 is high near the surface, shows a sharp decline at -30cm, and then steadily increases with depth. Conversely, K concentration in EU5 is lower near the surface and higher at depth, with a small peak occurring at -20cm and large spike at -40cm that is coincident with a peak in ^{238}U and ^{232}Th. Beta dose rates derived from radionuclide concentrations in the sediment are relatively consistent for most samples, with relative standard deviations of 20.5% in EU5 and 17.5% in EU6, averaging 23.4% overall. Gamma dose rates vary slightly more, with relative standard deviations of 21.9% in EU5 and 25% in EU6, altogether averaging 26.4%. Gamma and beta dose rates from NAA/DNC are generally higher in EU5 profile than EU6 profile, thus the total dose rates show the same trend. On average, NAA/DNC gamma dose rates are 38% higher and external NAA/DNC beta dose rates are 33% higher, resulting in total dose rates which are overall 17.5% higher. Cosmic radiation accounts for nearly half of the total external dose rate for most samples, and is actually dominant for three samples in EU6 (EU6-1, EU6-4, EU6-5), but slightly less significant in EU5 due to the higher concentration of radionuclides present.

Table 5. Dose rates determined using neutron activation analysis (NAA) and delayed neutron counting (DNC) for ^{238}U, ^{232}Th and K

Sample	Depth (cm)	^{238}U (ppm)[1]	^{232}Th (ppm)[1]	K (%)[1]	Moisture Content (%)[2]	Cosmic Dose Rate (μGy/a)[3]	External Beta Dose Rate (μGy/a)[4]	Gamma Dose Rate (μGy/a)[4]	Total Dose Rate (μGy/a)[5]
EU6-1	10	0.56 ± 0.1	0.65 ± 0.05	0.008568 ± 0.000687	2.3	252 ± 25	89.0 ± 12.3	94.3 ± 11.3	445.7 ± 16.9
EU6-2	20	0.69 ± 0.1	0.95 ± 0.07	0.008154 ± 0.000540	4.5	223 ± 22	108.8 ± 12.1	120.2 ± 11.3	462.4 ± 16.7
EU6-3	30	0.66 ± 0.1	0.77 ± 0.06	0.004573 ± 0.000451	5.2	211 ± 21	98.3 ± 12	107.2 ± 11.1	426.9 ± 16.5
EU6-4	40	0.50 ± 0.1	0.61 ± 0.05	0.005092 ± 0.000441	4.1	200 ± 20	76.9 ± 12.1	83.6 ± 11.1	370.9 ± 16.6
EU6-5	50	0.37 ± 0.1	0.58 ± 0.04	0.005634 ± 0.000415	3.1	194 ± 19	61.5 ± 12.2	68.8 ± 11.1	334.7 ± 16.7
EU6-6	60	0.62 ± 0.1	1.17 ± 0.07	0.007078 ± 0.000415	1.3	190 ± 19	107.6 ± 12.5	125.9 ± 11.6	433.9 ± 17.2
Average							90.4 ± 18.5	100 ± 21.9	412.4 ± 49.1
EU5-1	10	0.88 ± 0.1	1.81 ± 0.12	0.004476 ± 0.000560	2.7	252 ± 25	149.8 ± 12.5	182.1 ± 12.3	594.3 ± 17.7
EU5-2	20	0.72 ± 0.1	1.07 ± 0.07	0.005461 ± 0.000751	5.6	223 ± 22	111.9 ± 12.0	127.1 ± 11.2	472.4 ± 16.6
EU5-3	30	0.64 ± 0.1	0.90 ± 0.07	0.004359 ± 0.000872	7.8	211 ± 21	96.1 ± 11.7	108.5 ± 11.0	425.9 ± 16.2
EU5-4	40	0.89 ± 0.1	1.24 ± 0.09	0.007424 ± 0.000833	9.5	200 ± 20	132.2 ± 11.6	148.5 ± 11.1	491.1 ± 16.2
EU5-5	50	0.73 ± 0.1	1.08 ± 0.08	0.007066 ± 0.001155	9.3	194 ± 19	110.6 ± 11.6	125.0 ± 10.9	439.9 ± 16.1
Average							120.1 ± 21.0	138.± 28.3	484.7 ± 66.5

1. U, Th, and K values were determined by NAA (for Thorium and Potassium) and DNC (for Uranium) on sub-samples derived from the OSL samples prior to chemical treatments
2. Water content was calculated as a fraction of dry weight determined from laboratory measurements.
3. Cosmic dose rate value calculated using the instant accumulation model, which assumes the present sediment depth and an overburden density of 2 g/cm3
4. These beta and gamma dose rates were calculated based on U, Th, and K concentrations determined for each sample accounting for moisture values of the sample. All beta and gamma dose rates are based on an assumption of secular equilibrium in the U and Th decay chains.
5. Includes total internal dose rate of 10.3 ± 2.2 μGy/a

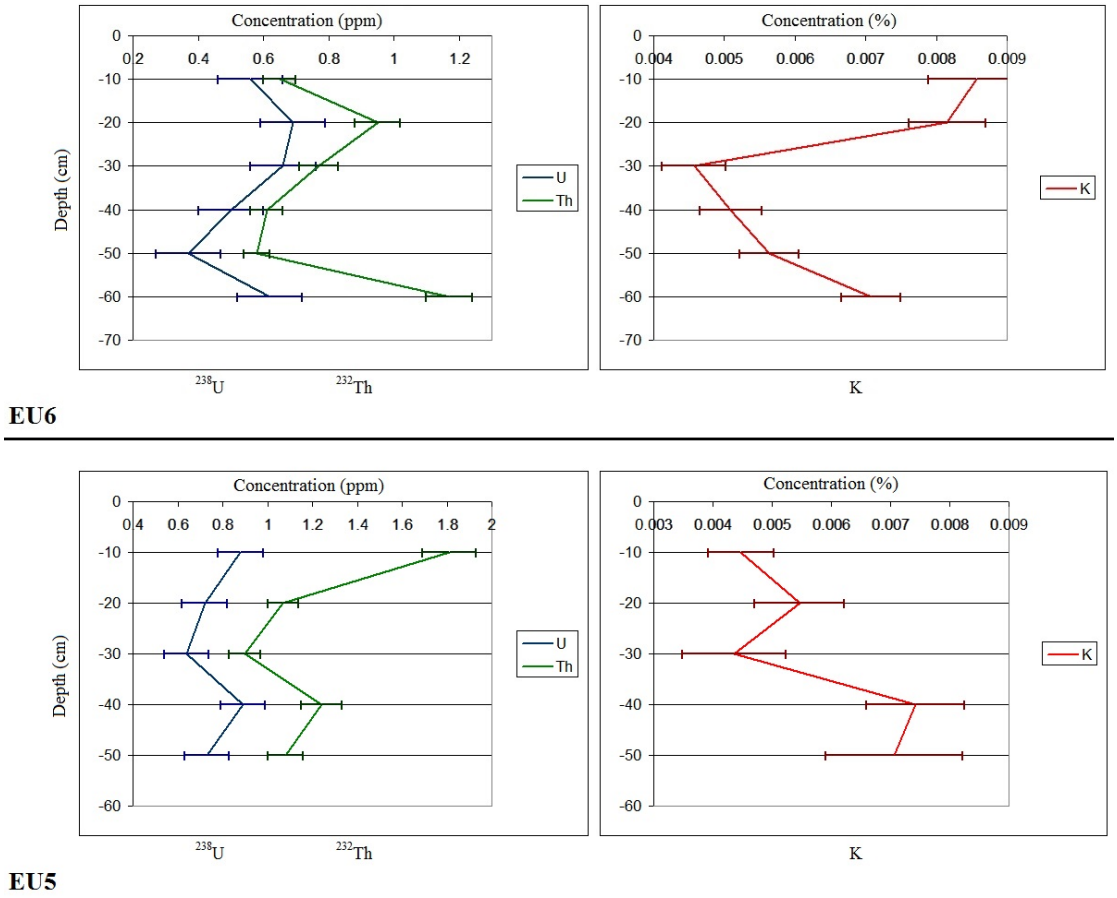

Figure 8. Radionuclide concentrations determined by neutron activation analysis (NAA) and delayed neutron counting (DNC) vs. depth below surface for both profiles studied.

5.3.2 Al_2O_3:C Dose Rates

The results from aluminum oxide dosimetry measurements are presented in Table 6. Using gamma dosimetry available for EU6-(1-5), Al_2O_3:C gamma dose rates are always higher than the corresponding gamma dose rates calculated from radionuclide concentrations determined by NAA and DNC (given in table 5). Conversely, when using Al_2O_3:C gamma dosimetry for EU5-(1-5), gamma dose rates are always lower than the corresponding gamma dose rates from NAA and DNC. Therefore, when applying Al_2O_3:C gamma dosimetry, the total dose rates are generally higher in the EU6 profile than in the EU5 profile. When Al_2O_3:C gamma + beta dosimetry is applied, beta dose rates are higher than the corresponding beta dose rates from derived from radioactive elements measured by NAA and DNC in almost all samples, with the exception of EU6-3 and EU6-5.

Negative beta dose values were reported by Al_2O_3:C dosimeters for EU6-3 and EU6-5, so zero doses were applied as an approximation for the beta dose rates. This may have occurred due to the placement of these dosimeters potentially between shells (as shells are commonly encountered in the midden), thus shielding the dosimeter from the surrounding beta radiation. Another possibility is that the sediment surrounding the aluminum oxide cylinder wrapped in electrical tape was composed purely of clean non-radioactive quartz grains, so no beta dose was received though it remained fully exposed to gamma radiation being delivered by more radioactive grains from afar. Given the inhomogeneity of the sediment, it is not unreasonable to suggest that the Al_2O_3:C dosimeter, by random placement in a complex matrix, could lie beyond the very limited reach of the unevenly distributed beta emitters. This would be considered a radiation "cold spot", and is the most likely cause for these two problematic results.

Overall, when applying Al_2O_3:C gamma + beta dosimetry, the total dose rates are again higher in the EU6 profile than the EU5 profile (on average 26% higher). The uppermost sample in both profiles have very high beta doses reported by Al_2O_3:Cbeta dosimetry (>500 uGy/a). For the EU5 profile, the difference in the total dose rates calculated from Al_2O_3:C gamma + beta dosimetry and Al_2O_3:C gamma + beta from NAA/DNC is minimal (generally within error). For the EU6 profile, however, the total dose rates calculated from Al_2O_3:C gamma + beta dosimetry and Al_2O_3:C gamma + beta from NAA/DNC are starkly different.

External gamma and beta dose rates based on the two different methods of calculation are graphically compared in Figure 9 and Figure 10. There is clearly no distinct relationship for the values reported by the two methods, as trend lines in the data for both beta and gamma dose rates are nearly perpendicular to the 1:1 relationship denoted by the dashed line. Only three samples were found to have dose rate values consistent within error between these two methods for both external beta and gamma dose rates (EU5-2,3,4). External beta and gamma dose rates determined from aluminum oxide dosimetry show a much higher variability than dose rates determined from NAA and DNC throughout the both profiles. External gamma dose rates have relative standard deviations of 52% and 43% in EU5 and EU6, respectively. External beta dose rates show even more variability, with relative standard deviations of 73% and 113% in EU5 and EU6, respectively.

Al_2O_3:C gamma dose rates in EU6 are much higher than in EU5, but similar to the those found in Harrison Ring (Rodrigues, 2015). NAA/DNC performed on an accidentally collected non-diagnostic sherd indicates that the pottery at this site is rich in U and Th, and thus seems to be an important contributor to the gamma doses. As such, gamma dose rates are quite logically higher in the middens than the mound, since they contain more broken pottery.

Table 6. Dose rates from Aluminum oxide (Al_2O_3:C) dosimeters

Dosimeter	Correspond-ing Sample	Depth (cm)	Beta + Gamma + Cosmic Dose Rate (μGy/a)[1]	Gamma + Cosmic Dose Rate (μGy/a)[2]	External Beta Dose Rate (μGy/a)	External Gamma Dose Rate (μGy/a)	Cosmic Dose Rate (μGy/a)[3]	Total Dose Rate (μGy/a)[4]
Stratigraphic Section								
HH1	EU6-1	10	975 ± 79	450 ± 67	525 ± 103	198 ± 71	252 ± 25	985.3 ± 79
HH2	EU6-2	20	644 ± 61	513 ± 76	131 ± 97	290 ± 79	223 ± 22	654.3 ± 61
HH3	EU6-3	30	436 ± 52	643 ± 94	-207 ± 107	432 ± 96	211 ± 21	653.3 ± 52
HH4	EU6-4	40	751 ± 66	328 ± 50	423 ± 83	128 ± 54	200 ± 20	761.3 ± 66
HH5	EU6-5	50	504 ± 55	525 ± 78	-21 ± 95	331 ± 80	194 ± 19	535.3 ± 55
-	EU6-6	60	-	-	-	-	190 ± 19	-
HH7	EU5-1	10	846 ± 72	270 ± 42	576 ± 83	18 ± 48	252 ± 25	856.3 ± 72
HH8	EU5-2	20	495 ± 55	315 ± 48	180 ± 73	92 ± 53	223 ± 22	505.3 ± 55
HH9	EU5-3	30	384 ± 50	280 ± 44	104 ± 66	69 ± 48	211 ± 21	394.3 ± 50
HH10	EU5-4	40	461 ± 53	328 ± 50	133 ± 73	128 ± 54	200 ± 20	471.3 ± 53
HH11	EU5-5	50	618 ± 60	271 ± 42	347 ± 73	77 ± 46	194 ± 19	628.3 ± 60

† for negative beta values reported by dosimeters, zero doses were applied as an approximation

1. Dose measured from dosimeters not encased in a stainless steel capsule
2. Dose measured from dosimeters encased in stainless steel capsules
3. Cosmic dose rate value calculated using the instant accumulation model, which assumes the present sediment depth and an overburden density of 2 g/cm^3
4. Includes total internal dose rate of 10.3 ± 2.2 μGy/a

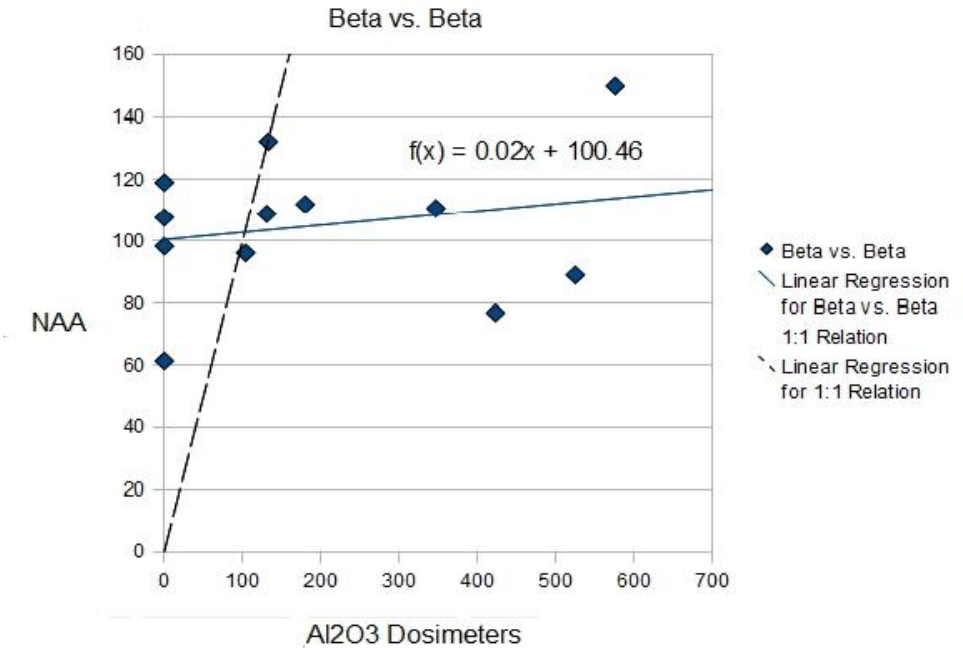

Figure 9. A comparison of the beta dose rates calculated from NAA/DNC against the beta dose rates recorded by Al_2O_3:C dosimeters.

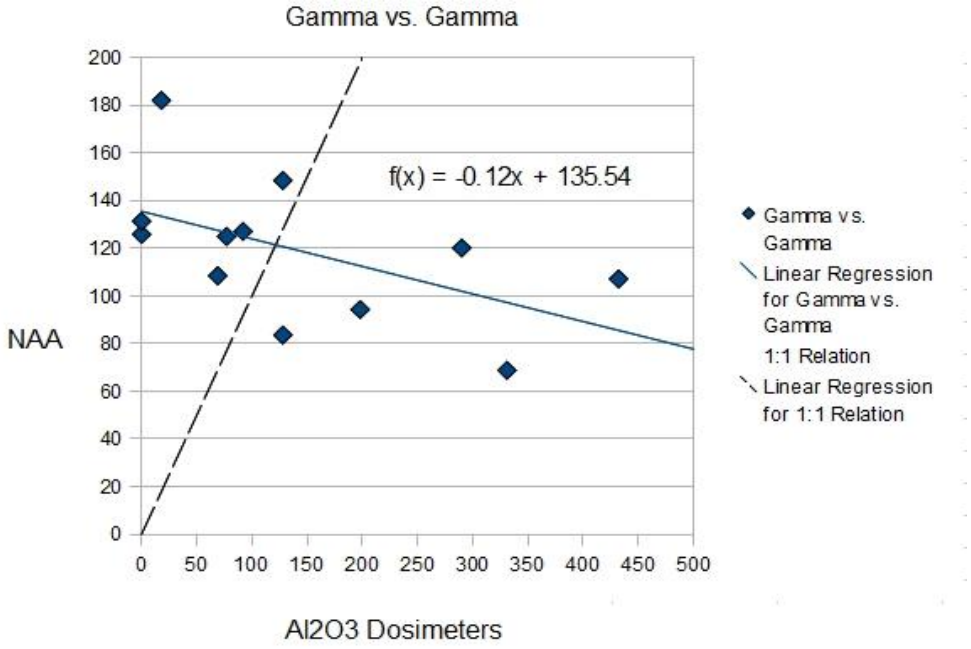

Figure 10. A comparison of the gamma dose rates calculated from NAA/DNC against the gamma dose rates recorded by Al_2O_3:C dosimeters.

5.4 OSL Ages

The samples studied here generally display high overdispersion and a positive skew in the observed equivalent dose distributions. As such, the 3-parameter minimum age model (MAM3, after Galbraith et al., 1999) was employed to isolate the correct burial dose. The central age model (CAM) was applied to just one sample (EU5-3) which exhibits relatively low overdispersion and insignificant skewness. Once the burial doses were ascertained, ages were calculated using three different methods of dosimetry:

1) External beta and gamma dose rates determined from NAA/DNC concentrations
2) External beta and gamma dose rates from Al_2O_3:C dosimetry
3) External beta dose rate determined from NAA/DNC concentrations and gamma dose rate from Al_2O_3:C dosimetry

The two profiles being studied lack significant age control, so there is little archaeological evidence to inform the correct selection of which technique to apply. Due to the inhomogeneity of the beta dose around most of the samples, and the fact that the volume of sediment extracted extends beyond the reach of beta radiation, there can be no certainty as to whether or not the sediment being dated was exposed to the same intensity of beta radiation as the dosimeters (which are quite small, thus only recording the beta dose rate accurately for a small, adjacent zone behind the sample being dated). As such, it is assumed that the best approximation of the true environmental dose rate in these samples is achieved by using a combination of the gamma dose rates from Al_2O_3:C dosimetry and the beta dose rates from the sediment itself reported by NAA/DNC. This is concurrent with the findings of Rodrigues (2015) where stronger age control in section was present, particularly in sediments containing widely-distributed, highly radioactive mineral grains. A similar situation was incurred in this study, especially in the sediments from EU5, so this method of dosimetry was selected as the preferred method for age calculations.

Since the Al_2O_3:C dosimeters corresponding to the sample EU6-6 were never recovered, this age was only calculated using the external dose rate derived purely from NAA/DNC elemental concentrations. Two very similar radiocarbon dates, 1130 ± 55 calBP and 1130 ± 85 calBP, from residue and soot on sherds recovered from the same levels as EU6-3 and EU6-4 are coincident with the ages calculated for these samples using external beta and gamma dose rates from Al_2O_3:C dosimetry. This indicates that the external dose rates may have been more accurately measured using just the Al_2O_3:C dosimeters for these two samples.

The results of OSL age calculations are presented in Table 7. These confirm the hypothesis that EU5 represents an earlier occupation, being deposited over approximately 400 years between 1928 +/- 372 and 1589 +/- 703 years ago. At this time, deposition began to occur in EU6, and continued for another 400 years (1511 +/- 372 to 1110 +/- 195 years ago). This profile was later capped by a recent non-archaeological deposit with an age of 340 +/- 115 years.

Table 7. Summary of paleodoses and age estimates for all samples using the various methods of dosimetry. Ages shown in Summary Table 8 correspond to those shown in bold here.

Sample Name/ Depth	Aliquot Diam.	Paleodose (Gy) (CAM)	Paleodose (Gy) (MAM)	Chosen Age Model	Age Estimate (yrs) (NAA/DNC)	Age Estimate (yrs) (γ from Dosimeters)	Age Estimate (yrs) (γ + β from Dosimeters)
EU 6-1 (10 cm)	0.5 mm	0.564 +/- 0.075	**0.187 +/- 0.06**	MAM	419 +/- 135	**340 +/- 115**	189 +/- 62
EU 6-2 (20 cm)	0.5 mm	0.763 +/- 0.026	**0.702 +/- 0.09**	MAM	1517 +/- 213	**1110 +/- 195**	1072 +/- 169
EU 6-3 (30 cm)	0.5 mm	0.813 +/- 0.053	**0.668 +/- 0.05**	MAM	1564 +/- 153	888 +/- 130	**1022 +/- 111**
EU 6-4 (40 cm)	0.5 mm	1.214 +/- 0.098	**0.773 +/- 0.12**	MAM	2083 +/- 350	1861 +/- 366	**1015 +/- 179**
EU 6-5 (50 cm)	0.5 mm	1.559 +/- 0.209	**0.902 +/- 0.19**	MAM	2694 +/- 590	**1511 +/- 372**	1684 +/- 390
EU 6-6 (60 cm)	0.5 mm	2.172 +/- 0.261	**0.868 +/- 0.19**	MAM	**2000 +/- 447**	-	-
EU 5-1 (10 cm)	0.5 mm	1.965 +/- 0.655	**0.684 +/- 0.30**	MAM	1150 +/- 501	**1589 +/- 703**	798 +/- 353
EU 5-2 (20 cm)	0.5 mm	1.494 +/- 0.365	**0.773 +/- 0.18**	MAM	1636 +/- 387	**1767 +/- 451**	1529 +/- 388
EU 5-3 (30 cm)	0.5 mm	**0.873 +/- 0.086**	0.650 +/- 0.19	CAM	2049 +/- 239	**2258 +/- 347**	2213 +/- 354
EU 5-4 (40 cm)	0.5 mm	1.259 +/- 0.121	**0.852 +/- 0.20**	MAM	1734 +/- 108	**1810 +/- 207**	1807 +/- 211
EU 5-5 (50 cm)	0.5 mm	0.953 +/- 0.057	**0.756 +/- 0.12**	MAM	1718 +/- 287	**1928 +/- 372**	1203 +/- 222

CHAPTER 6: DISCUSSION

6.1 Luminescence Characteristics

The OSL ages reported from Hare Hammock were obtained using measurements of quartz grains with 0.5 mm aliquots (~15 grains per aliquot). The results from dose recovery tests indicate that the quartz collected from this site demonstrates good luminescence behaviour. This is supported by replicability of measurement points on the dose response curves using test doses in the SAR protocol, and the proper form of the OSL decay curves. Dose recovery tests on single grains at the adjacent Harrison Ring site by Rodrigues (2015) evince that natural variations in luminescence properties of the quartz grains here can account for approximately 15% of the overdispersion in equivalent doses. Those single-grain measurements were also used to produce a cumulative light sum which indicated that 95% of the light sum produced by a 0.5mm aliquot is usually emitted from just 1-2 of the grains present on the disc. Since the two sites are literally side by side (and generally considered as one large complex), the quartz grains deposited at each are quite likely to have very similar luminescence properties. The OSL ages Rodrigues obtained when using both 0.5 mm aliquots and single grains were highly consistent, often statistically indistinguishable, which gives confidence in the accuracy of the 0.5 mm aliquot measurements used in this study at Hare Hammock.

6.2 Equivalent dose distributions and sources of scatter

The high level of D_E overdispersion observed in sediments at Hare Hammock (above what is expected based on measurements from dose-recovery tests on single grains by Rodrigues (2015)), along with the positive skew in their D_E distributions imply that the source of scattering is most likely external and not associated with variability in intrinsic luminescence characteristics. There is a multitude of potential external sources of equivalent dose scatter which have been discussed in the literature, such as partial or incomplete bleaching (e.g. Duller, 1994; Olley et al., 1998), post-depositional mixing of the sediment (e.g. Bateman et al., 2003, 2007), and heterogeneity in microdosimetry (e.g. Murray and Roberts, 1997; Vandenberghe et al., 2003). A minimum age model is usually applied to samples that demonstrate a large amount of scatter, such as the ones analyzed in this study. Based on the statistical analysis of D_E distributions, the most appropriate method to employ is a 3-parameter minimum age model (MAM3) for all samples in this report except one. As such, the minimum age model (MAM3) was used to isolate the youngest grain populations from the observed equivalent dose distributions for all samples but EU5-3. Only 7/48 aliquots were accepted for this sample, so it is quite possible and in fact likely that this small sampling does not accurately reflect the actual full range of equivalent doses present in the sample. Due to the low skewness in the data, which is also likely an artefact of the low number of accepted aliquots, the central age model (CAM) was applied to this sample.

The radiation environment in which the sediments at Hare Hammock are immersed has a dominant cosmic ray component, which accounts for ~25-60% of the total dose rates for the samples examined here. This attribute has been frequently observed in Florida sites where other OSL studies have taken place (eg. Rink and Lopez, 2010; Lopez, 2007; Thompson et al., 2007). Sediments composed primarily of quartz are known to have the potential to host a substantial amount of heterogeneity in beta dose rates, since the presence of even a small quantity of beta emitters, such as heavy minerals and feldspars, within the sediment can significantly affect the doses acquired by the surrounding non-radioactive quartz grains within the very limited reach of their beta radiation (Mayya et al., 2006; Chauhan and Singhvi, 2011). The results obtained from Al_2O_3:C dosimetry in the sediments at Hare Hammock indicate a notably heterogeneous beta radiation environment. The variations in beta dose-rates were not captured in most samples using neutron activation analysis and delayed neutron counting, which provide an averaged dose-rate for the entire volume of mixed sediment using a sub-sample of only 1 g (which might not be a truly representative fraction). The averaging of dose rates when using NAA/DNC obscures the high level of variability existing at small scales which can only be detected using in-situ Al_2O_3:C beta dosimetry.

The dosimetric measurements using Al_2O_3:C cylinders presented here are part of a pioneer study in applying this technique to a dating context. In a complex radiation environment like what was encountered at Hare Hammock, a combination of the NAA/DNC and Al_2O_3:C dosimetry results was found to be the most effective method for ascertaining environmental dose rates. This result is supported by the findings of the companion study by Rodrigues (2015) at Harrison Ring, which tested the same combination of dosimetric techniques in a section with firm independent age control. In both of these studies, the most appropriate method for determining dose rates is to use the beta dose calculated from NAA/DNC to represent a volumetric average throughout the sample, and gamma dosimetry reported by the in-situ Al_2O_3:C dosimeters, which provides an averaged dose from the surrounding 30 cm radius sphere within the sediment. In the EU5 profile, ages calculated using beta and gamma doses determined purely from NAA/DNC seem to be underestimated, as do most of the ages calculated using just the doses reported by Al_2O_3:C dosimeters. In contrast, ages calculated using only doses from NAA/DNC in the EU6 profile appear to be significantly overestimated, while most of the ages calculated using Al_2O_3:C dosimetry alone are reasonably similar to those calculated using the combined approach. The gamma dosimetry provided by Al_2O_3:C dosimeters should yield the most accurate gamma dose rate, as they record the dose being delivered from the full 30 cm range of gamma rays. When determining the beta dose rate, on the other hand, especially in such highly heterogeneous sediments, measurements based on a volumetric average should theoretically be the apposite technique to use. It is preferable over small-scale Al_2O_3:C dosimetry in this type of environment since the dose recorded by the dosimeter wrapped in electrical tape can be heavily influenced by the presence of radioactive hot or cool spots within just the 2 mm surrounding it.

A commonly suggested source of equivalent dose scatter is the post-depositional mixing of sediments via bioturbation. It has been implicated as a cause for the inaccuracy of OSL age estimations at a number of previously studied archaeological sites (eg. Bateman et al., 2007; Forrest et al., 2003; Rink et al., 2012a, b; Thulman, 2012; Wilder et al., 2007). Further studies of this process, conducted by Bateman et al. (2003) and Rink et al. (2013), have demonstrated that biological agents such as ants can transport sediment grains upward from lower, older units and deposit them in younger, shallow sediment layers. This is referred to as biomantling. Since these grains are not zeroed during transport in the sediment column, they can build up in a higher layer and cause significant scatter in dose distribution and produce ages, which are older than the true depositional age of the sample (Cunningham et al. 2011). It is equally possible for younger or even zero dose grains from the surface to be carried downward into older layers, making them appear younger. The post-depositional effects that bioturbation can impose on sediments has frequently been used to comprehend the incoherence between OSL and radiocarbon ages which is found at many archaeological sites in Florida (Wilder et al., 2007; Rink et al., 2012a, b). Since the effects of bioturbation appear to be so pervasive, it has warranted further study. A report by Bateman et al. (2007), which includes OSL results from four different sites, determined that high overdispersion and skewness in equivalent dose distribution, as well as populations of zero dose grains provide evidence that post-depositional disturbance has most likely taken place.

Equivalent dose scatter can also often be the result of incomplete bleaching before deposition, which is strongly dependant on the manner in which the sediments are deposited. Incomplete bleaching is most commonly associated with fluvial sediments since the amount of sunlight is diminished with water depth and turbidity (Olley et al., 1998). Anthropogenic deposits can also have incomplete or partial bleaching, but this depends on the process by which the sediments are accumulated. Unintentional or slow accumulation will likely result in complete or near complete bleaching, while sediments placed for constructive purposes could potentially have incomplete bleaching. This is mainly determined by the construction technique being used. For example, a sand-rich mound examined by Pluckhahn et al. (2015) was built upon a base of zone-filled sand which allowed it to be completely bleached as it was spread about. The rest of the mound, however, was built using basket loads of sand direct from their quarry, thus many of the grains were transported and re-deposited without being zeroed (i.e. incompletely bleached). As the sand was collected and transported, grains taken from the active quarry face would have a zero signal, but other grains scooped up from beneath the surface might not be completely bleached during transport. If the mounds at Hare Hammock were built in a similar fashion, then many of the grains would not receive sufficient light exposure before being redosited, thus retaining their pre-mining OSL dose. Since it is difficult to tell what method was actually used, age overestimations cannot be definitively attributed to this process.

At Hare Hammock, sedimentary deposition is largely dominated by aeolian processes, with some anthropogenic deposition. There is no sedimentary or geomorphological evidence indicating the occurrence of any fluvial activity. As such, the primary cause for equivalent dose scatter at this site is most likely the complexity of the beta-microdosimetry. Of course, it is also quite likely that some of the scatter is the result of post-depositional mixing. Because EU5 may represent a paleoindian mound construction, the possibility cannot be ruled out that some of the scatter could be due to incomplete bleaching, which is dependant on the technique used for construction. Nonetheless, the discrepancy between the results from Al_2O_3:C dosimetry and NAA/DNC strongly implicate variations in mircodosimetry as the dominant factor.

6.3 OSL age results

This study yielded a sediment accumulation history at Hare Hammock spanning from approximately 2000 years ago to about 340 years ago for one of the shallowest samples. Final age estimates are generally found to be in stratigraphic order, with the exception of EU6-2 and EU5-3, however, if the range of error in these samples and the ones directly underlying them is considered, they are statistically indistinguishable. The age from EU5-3 is probably overestimated by a notable amount, as this age was calculated using the central age model due to the small quantity of acceptable aliquots which do not likely provide an accurate representation of the true equivalent dose distribution (see discussion above). Likewise EU5-1 had too few aliquots accepted for a useful MAM3 determination, and therefore yielded a very large age uncertainty, which is difficult to attribute to a given cultural period.

The two profiles studied represent two sequential paleoindian occupations. The EU5 profile in the smaller Hare Hammock mound shows a chronology spanning from over 1900 to less than 1600 years ago, consistent with Early Swift Creek through to Late Swift Creek or very early Weeden Island. This agrees with the expectation that this was a Swift Creek construction, as this mound is believed to be the burial mound associated with the nearby Harrison Ring, both of which produced almost exclusively Swift Creek ceramics. Table 8 shows the selected age estimate for each sample along with the cultural period that they are consistent with. The EU6 profile in the Hare Hammock ring provides a chronology that seems to follow after that of EU5. The lowermost sample (EU6-6) produced an age which seems to be pre-archaeological, but this age was calculated using purely NAA/DNC dosimetry since the corresponding dosimeter was not recovered, so it is likely an overestimate. Above this, EU6-5 provided an age of 1511 +/- 372 years, which is remarkably close to the age of the uppermost sample from EU5 (1589 +/- 703 years), notwithstanding the large uncertainty in the latter age. This marks the point in time at which the Weeden Island descendents choose to abandon the earlier Swift Creek mound and ring in order to begin another larger settlement (the larger Hare Hammock mound and ring). This is again consistent with archaeological expectations as such

practices became prominent with the emergence of Weeden Island culture. Occupation of this new settlement seems to have lasted the next 400 years, based on the age of 1110 +/- 195 years yielded from EU6-2. This relates to Early through to Late Weeden Island, which is in agreement with the artifacts and radiocarbon dates recovered from this site. The shallowest sample from EU6 produced an age of 340 +/- 115 years, and likely represents aeolian sedimentation atop the midden long after the site was abandoned.

Table 8. Summary of the selected age estimates for each sample and related cultural period.

Sample Name/ Depth	Paleodose (Gy)	Age Estimate (yrs)	Consistent with
EU 6-1 (10 cm)	0.187 +/- 0.06	340 +/- 115	Recent – non-archaeological
EU 6-2 (20 cm)	0.702 +/- 0.09	1110 +/- 195	Late Weeden Island
EU 6-3 (30 cm)	0.668 +/- 0.05	1022 +/- 111	Late Weeden Island
EU 6-4 (40 cm)	0.773 +/- 0.12	1015 +/- 179	Late Weeden Island
EU 6-5 (50 cm)	0.902 +/- 0.19	1511 +/- 372	Early Weeden Island
EU 6-6 (60 cm)	0.868 +/- 0.19	2000 +/- 447	Probable overestimate, no dosimeter
Mean +/- 1σ EU 6-2, 6-3, 6-4		**1049 +/- 43**	Late Weeden Island
EU 5-1 (10 cm)	0.684 +/- 0.30	1589 +/- 703	Too few aliquots to estimate cultural period
EU 5-2 (20 cm)	0.773 +/- 0.18	1767 +/- 451	Early Swift Creek
EU 5-3 (30 cm)	0.873 +/- 0.086	2258 +/- 347	Probable age overestimate, too few aliquots
EU 5-4 (40 cm)	0.852 +/- 0.20	1810 +/- 207	Early Swift Creek
EU 5-5 (50 cm)	0.756 +/- 0.12	1928 +/- 372	Early Swift Creek (no Deptford artifacts)
Mean +/- 1σ EU 5-2, 5-4, 5-5		**1835 +/- 68**	Early Swift Creek

Only two of the samples in this study had radiocarbon dates corresponding to the same stratigraphic levels. These relate to EU6-3 and EU6-4, which produced calibrated radiocarbon ages of 1130 +/- 55 years CalBP and 1130 +/- 85 years CalBP from residue and soot off Wakulla Check Stamped and Carrabelle pottery sherds, respectively. As the ages calculated for these samples using only Al_2O_3:C dosimetry (1022 +/- 111 years for EU6-3 and 1015 +/- 179 years for EU6-4) both lie within error of these radiocarbon dates, it seems evident that the beta microdosimetry may have been more accurately recorded by the dosimeters than could be obtained from a volumetric analysis of the sediment alone. This could be due to the influence of pottery on the sample, which is not captured by NAA/DNC since only the sediment is analyzed. As such, the concordance with radiocarbon dates indicates that, for just these two samples, the most appropriate method to apply for age calculations is to use the dose rates exclusively from Al_2O_3:C dosimetry. Although these ages are likely to be underestimated slightly, they still provide the most sensible results. Irregardless, the congruency of almost all OSL ages with previous archaeological expectations leads us to believe that the most effective method to use for all other samples is the combined NAA/DNC and Al_2O_3:C dosimetric technique.

It is possible to combine ages in each unit based on the quality of the data and the attribution to cultural periods in order to calculate mean ages (Table 8). Uncertainties associated with these mean ages are a representation of the variation from the mean rather than the mean age error. For EU5 we find a mean age of 1835 +/- 68 a corresponding to the Early Swift Creek Period. This is entirely consistent with expectation since this unit is interpreted to be a Swift Creek construction, as this mound is believed to be the burial mound associated with the nearby Harrison Ring, both of which produced almost exclusively Swift Creek ceramics. For EU6, we find a mean age of 1049 +/- 43 a, corresponding to the Late Weeden Island period. This overlies a single age of 1511 +/- 372 a corresponding to the Early Weeden Island Period. This unit is within the Hare Hammock Mound and Ring, which were apparently occupied later and are rich in Weeden Island ceramics.

There is one problematic radiocarbon date originating from 30cm below EU5-5, coming from the residue adhered to a Swift Creek Complicated Stamped pottery sherd, which returned an age of 1450 +/- 80 years calBP. This appears to postdate the overlying sediment, however, the sample may have been contaminated by modern carbon in the section, thus causing the measured radiocarbon age to be too young. A study by Stott et al. (2001) has shown that contamination with modern carbon can account for hundreds of years of variation in radiocarbon dates obtained from residues adhered to pottery from various archeological sites in England. This exemplifies the general veracity OSL dating over radiocarbon dating, which has multiple disadvantages. For one, radiocarbon dating relies on the availability of an organic material, while OSL dating is applied to quartz grains which are nearly ubiquitous in most archaeological deposits, especially in Florida. Radiocarbon dates must also be converted to a calendar date using a calibration based on the isotopic conditions of the "carbon reservoir" from which the material being dated

incorporated its carbon (Ascough et al., 2005). The use of OSL eliminates the uncertainties associated with modern carbon contamination and the estimation of the reservoir effects of a given location. Studies using a combination of OSL and ^{14}C, such as Bateman et al. (2008), emphasize the need for further investigation of the reservoir effects of local sites. The research of Stone et al. (2003) also demonstrates the value of applying OSL when contamination of radiocarbon samples is suspected. An additional advantage is that OSL dates the actual deposition event, while radiocarbon dates reflect the point in time when the material stopped incorporating new carbon, which is not necessarily coincident with the time of its deposition, or re-deposition. OSL dating is, however, more costly and time consuming than radiocarbon dating, especially when using dosimeters which must be left in place for nearly a year. A trained individual is required to visit the site, as more care must be taken when sampling, and return a second time to recover dosimeters. Radiocarbon dating is a quicker, cheaper method and is ideal for preliminary studies, while OSL can be employed if a deeper investigation is desired. The most effective approach is always to use multiple dating methods when possible, since coherent independent dates are the most reliable.

The only downfall of OSL ages reported in this study is the relatively large errors when compared to the precision of the radiocarbon dates. Overall, errors associated with OSL ages range from 11-44% with an average of 22%. Excluding the two uppermost samples, which have notably higher errors appended, the average error drops to 18% with a range of 11-25%. This is significantly greater than the error terms associated with the radiocarbon dates at this site, which range from ~5-8%. The large errors reported here are not the result of intrinsic OSL properties, but can be attributed to the complexity of the microdosimetry which characterizes the sediments at this site, particularly the severe heterogeneity observed in beta dose rates. Nevertheless, the mean ages have much reduced uncertainties relative to individual age uncertainties.

CHAPTER 7: CONCLUSIONS

This study successfully determined OSL ages at Hare Hammock in two profiles which represent two subsequent paleoindian occupations. These results conform to the hypothesis that the EU5 profile in the smaller Hare Hammock mound represents an earlier occupation, with a mean age of 1835 +/- 68 years, consistent with Early Swift Creek. This is in agreement with the archaeological expectation that this was a Swift Creek construction, as it is believed to be the burial mound associated with the nearby Harrison Ring since both of these produced almost exclusively Swift Creek ceramics. The strikingly similar ages from EU5-1 and EU6-5 (1589 +/- 703 years and 1511 +/- 372 years) likely correspond to the abandonment of the Swift Creek site and the establishment of the Weeden Island settlement. This cannot be said with complete certainty as the former age bears a large error, making it difficult to assign to a particular cultural period. The later occupation examined at EU6 was found to have a mean age of 1049 +/- 43 years, which corresponds with the Late Weeden Island period. This overlies a single age of 1511 +/- 372 years, which relates to the Early Weeden Island period. The chronology obtained from these OSL ages is in agreement with the artifacts and radiocarbon dates recovered from this site.

As part of the development of the application of Al_2O_3:C dosimetry, ages were calculated using three different methods of dosimetry. The best approximation of the true environmental dose rate in these samples was found to be attained by the use of a combination of the gamma dose rates from Al_2O_3:C dosimetry and the beta dose rates from the sediment reported by NAA/DNC. This combined technique seems to provide the most comprehensive dose rates when dating sediments in a heterogeneous beta radiation environment such as those encountered at Hare Hammock. Small scale variations in beta dose-rates were only detectable when using in-situ Al_2O_3:C beta dosimetry, as they are obscured by the averaging effect when using NAA/DNC. However, when determining beta dose rates for age calculations, measurements based on NAA/DNC are more suitable than small-scale Al_2O_3:C dosimetry since the beta dose can be strongly influenced by radioactive hot or cool spots within the 2 mm surrounding the dosimeter.

Some of the ages may have been slightly overestimated as a result of incomplete bleaching due to the effects of anthropogenic construction, more so the ages from EU5 because it is believed to represent the Smaller Hare Hammock Mound. However, these effects were minor and do not seem to have been problematic, as all ages are in agreement with radiocarbon dates and ceramic chronology from the site. The relatively large uncertainties associated with the OSL ages are primarily caused by the wide scatter which can sufficiently be explained by variations in beta microdosimetry.

The significance of this study is that it successfully employed OSL dating to provide a chronology for the habitation of Swift Creek and Weeden Island sites. It is only

the second time that this has been attempted for a Swift Creek site and the first time for a Weeden Island site. Although the OSL ages of individual samples carry large uncertainties, it is important to note that the mean ages determined from each profile have very low uncertainties associated with them, comparable to that achieved by calibrated radiocarbon dates at the site. This latter finding also contributes to the significance of the findings, because it has been shown that OSL can achieve small uncertainties in these types of environments, enabled only by doing high resolution sampling, which also provides insight on the complex dosimetry environment and a tighter chronology. The value of taking multiple samples from each vertical section is especially well demonstrated here, as the entirety of the two occupations seems to have been captured and the mean ages for both profiles are in excellent agreement with radiocarbon dates and archaeological evidence. The success of these age estimations relies on the proper use of Al_2O_3:C dosimetry, which was applied for just the second time to the dating of sediments. The results of this study are quite gratifying because, in spite of the difficulties encountered, the ages obtained are within the accepted range for Swift Creek and Weeden Island cultures and concordant with archaeological expectations for the two occupations, verifying the merit of applying OSL dating in these types of deposits.

References:

Aitken, M. (1998). An introduction to optical dating: the dating of Quaternary sediments by the use of photon-stimulated luminescence. Oxford: Oxford University Press.

Adamiec, G., & Aitken, M. (1998). Dose-rate conversion factors: update. *Ancient TL*, *16*(2), 37–50.

Antoine, P., Rousseau, D.D., Zöller, A., Lang, L., Munaut, A.V., Hattè, C., Fontugne, M., (2001). High-resolution record of the last Interglacial-glacial cycle in the Nussloch loess-palaeosol sequences, Upper Rhine Area. Germany. *Quaternary International, 76/77*, 211–229.

Ascough, P., Cook, G., & Dugmore, A. (2005). Methodological approaches to determining the marine radiocarbon reservoir effect. Progress in Physical Geography, 29 (4), 532-547.

Bailey, R. M., & Arnold, L. J. (2006). Statistical modelling of single grain quartz D_e distributions and an assessment of procedures for estimating burial dose. *Quaternary Science Reviews*, *25*(19), 2475-2502.

Bateman, M.D., Carr, A.S., Murray-Wallace, C.V., Roberts, D.L., & Holmes, P.J. (2008). A dating intercomparison study on Late Stone Age coastal midden deposits, South Africa. *Geoarchaeology*, 23 (6), 715-741.

Bateman, M.D., Frederick, C.D., Jaiswal, M.K. & Singhvi, A.K. (2003). Investigations into the potential effects of pedoturbation on luminescence dating. *Quaternary Science Reviews, 22*, 1169–1176.

Bateman, M.D., Boulter, C.H., Carr A.S., Frederick, C.D., Peter, D., Wilder, M. (2007). Preserving the palaeoenvironmental record in drylands: bioturbation and its significance for luminescence-derived chronologies. *Sedimentary Geology, 195*, 5–19.

Brose, David S., and George W. Percy (1974). An Outline of Weeden Island Ceremonial Activity in Northwest Florida. Paper presented at the 39th Annual Meeting of the Society for American Archaeology, Washington.

Bøtter-Jensen, L., McKeever, S.W.S, Wintle, A.G. (2003). Optically Stimulated Luminescence Dosimetry. Elsevier, Amsterdam.

Chauhan, N, Singhvi, A.K. (2011). Distribution of SAR paleodoses due to spatial heterogeneity of natural beta dose. *Geochronometria,* 38, 190–198

Cunningham, A. C., Wallinga, J., & Minderhoud, P. S. (2011). Expectations of scatter in equivalent-dose distributions when using multi-grain aliquots for OSL dating. *Geochronometria*, *38* (4), 424-431.

Duffee, E.M., Baldwin, R.A., Lewis, D.L., Warmack, W.B. (1984). Soil survey of Bay County, Florida. U.S. Department of Agriculture, Soil Conservation Service. Washington, DC.

Duller, G.A.T. (2008). Luminescence dating: Guidelines on using luminescence dating in archaeology. English Heritage, 1-43.

Duller, G.A.T. (1994). Luminescence dating of poorly bleached sediments from Scotland. *Quaternary Geochronology, 13*, 521–524.

Feathers, J.K. (1997). The application of luminescence dating in American Archaeology. J*ournal of Archaeological Method and Theory*, 4 (1), 1-66.

Feathers, J.K. (2003). Use of luminescence dating in archaeology. *Measurement Science and Technology*, 14 (9), 1493-1509.

Forrest, B., Rink, W.J., Bicho, N., Ferring, C.R. (2003). OSL ages and possible bioturbation signals at the Upper Paleolithic site of Lagoa do Bordoal, Algarve, Portugal. *Quaternary Science Reviews, 22*, 1279–1285.

Galbraith, R.F.,Roberts, R.G., Laslett, G.M.,Yoshida, H., Olley, J.M. (1999). Optical dating of single and multiple grains of quartz from jinmium rock shelter, northern Australia, Part 1: experimental design and statistical models. *Archaeometry, 41*, 339-364.

Galbraith, R.F., & Roberts, R.G. (2012). Statistical aspects of equivalent dose and error calculation and display in OSL dating: an overview and some recommendations. Quaternary *Geochronology*, 11, 1-27.

Galbraith, R. F., Roberts, R. G., & Yoshida, H. (2005). Error variation in OSL palaeodose estimates from single aliquots of quartz: a factorial experiment. *Radiation Measurements, 39*(3), 289–307.

Guérin, G., Mercier, N., Adamiec, G. (2011). Dose-Rate Conversion Factors: Update.

Ancient TL, 29(1): 5-8.

Kalchgruber, R., & Wagner, G. A. (2006). Separate assessment of natural beta and gamma dose-rates with TL from a-Al2O3: C single-crystal chips. *Radiation Measurements*, *41*, 154–162.

Lopez, G. (2007). Optical dating of barrier islands in the Gulf of Mexico. Ancient TL – published theses. http://www.aber.ac.uk/ancient-tl/.

López, G.I., & Rink, W.J. (2007). Characteristics of the burial environment related to quartz SAR-OSL dating at St. Vincent Island, NW Florida, U.S.A. *Quaternary Geochronology*, 2, 65-70.

Mayya, Y.S., Morthekai, P., Murari, M.K., Singhvi, A.K. (2006). Towards quantifying beta microdosimetric effects in single-grain quartz dose distribution. *Radiation Measurements, 41,* 1032-1039.

Mejdahl, V., & Christiansen, H.H. (1994). Procedures used for luminescence dating of sediments. *Quaternary Science Reviews*, 13 (5-7), 403-406.

Mejdahl, V. (1979). Thermoluminescence dating: beta-dose attenuation in quartz grains. *Archaeometry, 21,* 61–72.

Mercier, N., Gaugez, C. (2012). ANATOL v. 2.0.52 [computer software]. LSCE – Domaine du CNRS, Gif-sur-Yvette, France.

Milanich, J. (1994). Archaeology of Precolumbian Florida. Gainesville: University Press of Florida.

Moore, C.B. (1902). Certain Aboriginal Remains of the Northwest Florida Coasts, Part II. *Journal of the Academy of Natural Sciences of Philadelphia, 12,* 128-358.

Moore, C.B. (1918). The *Northwestern Florida Coast Revisited. Journal of the Academy of Natural Sciences of Philadelphia, 16,* 514-580.

Murray, A.S., Roberts, R.G. (1997). Determining the burial time of single grains of quartz using optically stimulated luminescence. *Earth Science Planetary Letters, 152,* 163–180.

Murray, A.S, Wintle, A.G. (2000). Luminescence dating of quartz using an improved single-aliquot regenerative-dose protocol. *Radiation Measurements, 32,* 57-73.

Murray, A.S., Wintle, A.G. (2003). The single aliquot regenerative dose protocol:

potential improvements in reliability. *Radiation Measurements, 37,* 377-381.

Olley, J.M., Caitcheon, G.G., Murray, A.S. (1998). The distribution of apparent dose as determined by optically stimulated luminescence in small aliquots of fluvial quartz: implications for dating young sediments. *Quaternary Science Reviews, 17,* 1033–1040.

Pluckhahn, T.J., Hodson, A.D., Rink, W.J., Thompson, V.D., Hendricks, R.R., Doran, G., Farr, G., Cherkinsky, A., Norman, S.P. (2015). Radiocarbon and Luminescence Age Determinations on Mounds at Crystal River and Roberts Island, Florida, USA. *Geoarchaeology*, 30(3), 238-260.

Polf, J. C., McKeever, S. W. S., Akselrod, M. S., Holmstrom, S. (2002). A real-time, fibre optic dosimetry system using Al_2O_3 fibre. *Radiation Protection Dosimetry*, 100, 301–304.

Prescott, J. R., Hutton, J. T. (1988). Cosmic Ray and Gamma Ray Dosimetry for TL and ESR. *Nuclear Tracks and Radiation Measurements*, *14*(1/2), 223–227.

Rhodes, E. J. (2011). Optically Stimulated Luminescence Dating of Sediments over the Past 200,000 Years. *Annual Review of Earth and Planetary Sciences*, *39*(1), 461–488.

Rink, W.J. (2001). Beyond ^{14}C Dating: A user's guide to long-range dating methods in archaeology. In Goldberg, P., Holliday, V.T., & Ferring, C.R. (Eds.) Earth Sciences and Archaeology (pp. 385-417). New York: Kluwer Academic/Plenum Publishers.

Rink, W.J., Odom, A.L. (1991). Natural alpha recoil particle radiation and ionizing radiation sensitivities in quartz detected with EPR: implication for geochronometry. *Nuclear Tracks and Radiation Measurements, 18*, 163–173.

Rink, W. J., Dunbar, J. S., Burdette, K. E. (2012a). The Wakulla Springs lodge site (8Wa329): 2008 excavations and new OSL dating evidence. *Florida Anthropological Society*, *65*(1-2), 5–23.

Rink, W. J., Dunbar, J. S., Doran, G. H., Frederick, C., Gregory, B. (2012b). Geoarchaeological investigations and OSL dating evidence in an archaic and paleoindian context at the Helen Blazes Site (8Br27), Brevard County, Florida. *Florida Anthropological Society*, *65*(1-2), 87–107.

Rink, W.J., Dunbar, J.S., Tschinkel, W.R., Kwapich, C., Repp, A., Stanton, W., Thulman, D.K. (2013). Subterranean transport and deposition of quartz by ants in sandy sites relevant to age overestimation in optical luminescence dating. Journal of Archaeological Science, 40 (4), 2217-2226.

Rodrigues, K. (2015). OSL Dating of a Coastal Swift Creek Occupation at Harrison Ring, Bay County, Florida. *Unpublished MSc Thesis,* McMaster University.

Russo, M., Hadden, C.S., Dengel, C. (2009). Archaeological investigations of mounds and ring middens at Hare Hammock – Tyndall Air Force Base. Southeast Archaeological Center National Park Service.

Russo, Michael, and Craig Denge (2009). Investigations at 8BY31 The Smaller Mound at Hare Hammock. Submitted to Tyndall AFB by the Southeast Archeological Center, National Park Service, under Work Order 47044. Ms. on file, SEAC, Tallahassee.

Russo, M., Dengel, C. and Shanks, J. (2012). Public Plazas as Mediating Loci at Weeden Island Coastal Settlements. Paper presented at the annual meeting of the Society for American Archaeology, Memphis.

Russo, M., Dengel, C., Shanks, J., McFeaters, A. (2014). Archaeological determinations of boundaries and cultural affiliations at the Hare Hammock 8By31 site. Southeast Archaeological Center National Park Service.

Sears, William H. (1973). The Sacred and Secular in Prehistoric Ceramics. In Variation in Anthropology: Essays in Honor of John C. McGregor, edited by Donald W. Lathrap and Jody Douglas, pp. 31-42. Illinois Archaeological Survey, Urbana.

Schwarcz, H.P. (2002). Chronometric dating in archaeology: A review. A*ccounts of Chemical Research*, 35 (8), 637-643.

Stone, T. and Cupper, M.L., (2003). Last Glacial Maximum ages for robust humans at Kow Swamp, southern Australia. *Journal of Human Evolution*, 45, 99-111.

Stott, A.W., Berstan, R., Evershed, P., Hedges, R.E.M., Ramsey, C.B., and Humm, M.J. (2001). Radiocarbon dating of single compounds isolated from pottery cooking vessel residues. *Radiocarbon*, *43*(2; PART A), 191-198.

Thompson, J., Jack Rink, W., & López, G. I. (2007). Optically stimulated luminescence age of the Old Cedar midden, St. Joseph Peninsula State Park, Florida. *Quaternary Geochronology*, *2*(1-4), 350–355.

Thulman, D. K. (2012). Bioturbation and the Wakulla Springs lodge site artifact distributions. *The Florida Anthropologist*, *65*(1-2), 25–34.

Vandenberghe, D., Hossain, S.M., De Corte, F., Van den haute, P., 2003. Investigations on the origin of the equivalent dose distribution in a Dutch cover sand. *Radiation Measurements,* 37, 433-439.

Wilder, M., Frederick, C.D., Bateman, M.D., Peter, D.E. (2007). Geoarchaeological investigations in the flats of the Osceola Plain, Highlands and Polk Counties, Florida. *The Florida Anthropologist, 60*, 97-116.

Willey, G.R. (1949). Archaeology of the Florida Gulf Coast. Smithsonian Miscellaneous Collections 115. Washington, D.C. Reprinted by University Press of Florida, Gainesville, 1998.